TECHNICAL MEMORANDUM

X-332-1

AERODYNAMIC CHARACTERISTICS AT MACH NUMBER 2.05 OF A SERIES OF HIGHLY SWEPT ARROW WINGS EMPLOYING VARIOUS DEGREES OF TWIST AND CAMBER

By Harry W. Carlson

Langley Research Center
Langley Field, Va.

NATIONAL AERONAUTICS AND SPACE ADMINISTRATION
WASHINGTON

October 1960
Declassified September 1, 1961

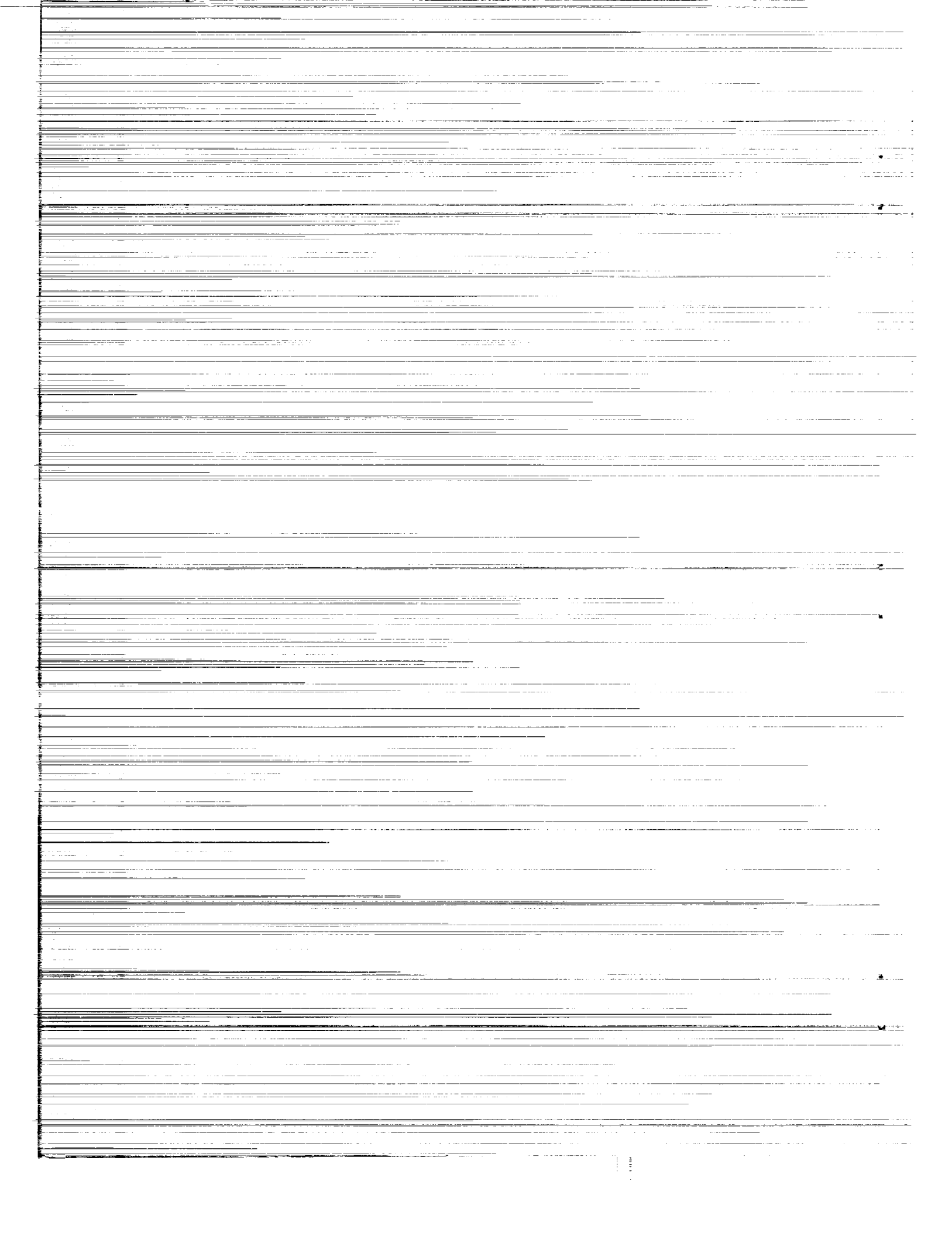

NATIONAL AERONAUTICS AND SPACE ADMINISTRATION

TECHNICAL MEMORANDUM X-332

AERODYNAMIC CHARACTERISTICS AT MACH NUMBER 2.05 OF A SERIES OF HIGHLY SWEPT ARROW WINGS EMPLOYING VARIOUS DEGREES OF TWIST AND CAMBER

By Harry W. Carlson

SUMMARY

A series of arrow wings employing various degrees of twist and camber were tested in the Langley 4- by 4-foot supersonic pressure tunnel. Aerodynamic forces and moments in pitch were measured at a Mach number of 2.05 and at a Reynolds number of 4.4×10^6 based on the mean aerodynamic chord. Three of the wings, having a leading-edge sweep angle of 70° and an aspect ratio of 2.24, were designed to produce a minimum drag (in comparison with that produced for other wings in the family) at lift coefficients of 0, 0.08, and 0.16. A fourth and a fifth wing, having a 75° swept leading edge and an aspect ratio of 1.65, were designed for lift coefficients of 0 and 0.16, respectively.

A 70° swept arrow wing with twist and camber designed for an optimum loading at a lift coefficient considerably less than that for maximum lift-drag ratio gave the highest lift-drag ratio of all the wings tested - a value of 8.8 compared with a value of 8.1 for the corresponding wing without twist and camber. Two twisted and cambered wings designed for optimum loading at the lift coefficient for maximum lift-drag ratio gave only small increases in maximum lift-drag ratios over that obtained for the corresponding flat wings. However, in all cases, the lift-drag ratios obtained were far below the theoretical estimates.

INTRODUCTION

It has long been recognized that because of their low zero-lift wave drag and low drag due to lift, highly swept arrow wings have the potential of allowing supersonic airplanes to compete successfully with the best subsonic airplanes in the critical matter of range (refs. 1 and 2).

However, if the maximum theoretical benefits are to be approached, it is necessary that a flat wing realize a high degree of the theoretically predicted leading-edge suction or that the wing be twisted and cambered to produce a theoretically optimum loading distribution.

The prediction of the leading-edge suction stems from the singularities in local velocities at the wing leading edge given by linearized theory. The existence of any large portion of the theoretical leading-edge suction has not been found in experiments.

It has been shown theoretically (refs. 3 and 4) that drag-due-to-lift factors slightly below those of the flat wing with full leading-edge suction can be achieved by producing an optimum loading distribution through the warping of the wing surface. It is significant that in this case, no leading-edge suction is demanded. The present paper will be concerned with the attainment of high lift-drag ratios through this latter approach.

For this optimum-loading-distribution method to succeed, it is imperative to avoid shocks and separated flow regions which would upset the balance between the local pressures and the slope of the surfaces on which they act. It is believed that in all the experimental work to date, these effects have been present to some degree at the lift coefficient required for the maximum lift-drag ratios. Experimental results for twisted and cambered wings have shown improvements over the corresponding flat wing, but have failed to reach the full theoretical benefits. (See refs. 5, 6, and 7.)

As noted in reference 1, the transonic flow phenomena (local shocks and regions of separated flow) may occur on the wing upper surface when the component of flow perpendicular to the wing leading edge reaches the speed of sound, even though the total velocity is greater than the speed of sound. In order to keep the perpendicular component of flow below sonic speed for the design lift condition, the leading-edge sweep angle must increase rapidly with Mach number. At speeds approaching the hypersonic range, the required sweeps would result in impracticably slender wings resembling bodies more than conventional wings.

Since at a Mach number of 2 the theoretical advantages of twist and camber are substantial and, at the same time, the planform restrictions are not unreasonable, several wings were designed for this Mach number to investigate the possibility of attaining the theoretical benefits. The design procedure used was adapted to these purposes by using computation techniques developed by Clinton E. Brown and Francis E. McLean of the Langley Research Center from the methods presented in references 8 and 9.

Three of the five half-span wings tested in the Langley 4- by 4-foot supersonic pressure tunnel at a Mach number of 2.05 had a leading-edge sweep of 70° and an aspect ratio of 2.24. One of these wings was twisted and cambered for a design lift coefficient of 0.16, a second wing employed only half that amount of twist and camber, and a third wing had no twist and camber. The remaining two wings had a 75° leading-edge sweep and an aspect ratio of 1.65. One of these wings had twist and camber corresponding to a design lift coefficient of 0.16 whereas the other wing had no twist and camber.

SYMBOLS

$b/2$	wing semispan
$\bar{c}$	wing mean aerodynamic chord
C_A	axial-force coefficient, $\frac{\text{Axial force}}{qS}$
C_D	drag coefficient, $\frac{\text{Drag}}{qS}$
$C_{D,o}$	drag coefficient at zero lift for uncambered and untwisted wings
C_L	lift coefficient, $\frac{\text{Lift}}{qS}$
C_m	moment coefficient about $\frac{\bar{c}}{4}$, $\frac{\text{Pitching moment}}{qS\bar{c}}$
C_p	pressure coefficient
l	overall length of wing measured in streamwise direction
L/D	lift-drag ratio, C_L/C_D
M	free-stream Mach number
q	free-stream dynamic pressure
R	free-stream Reynolds number based on mean aerodynamic chord
S	wing area, half-span model
U	free-stream velocity

u,v perturbation velocities in x- and y-directions

x,y,z Cartesian coordinate system with origin at wing apex, X-axis streamwise

b', c', x', y', θ' coordinates used in defining mean camber surfaces (fig. 3)

α angle of attack, deg

Λ leading-edge sweepback angle, deg

Subscripts:

max maximum

min minimum

MODELS AND INSTRUMENTATION

Photographs of the five half-span models (designated wings 1 to 5) mounted on the boundary-layer bypass plate are shown in figure 1. The first three wings had a 70° swept leading edge and an aspect ratio of 2.24. Each of the wings in this first series was designed to produce a minimum drag (in comparison with that produced for other wings in the family) at a certain lift coefficient. These design lift coefficients are 0, 0.08, and 0.16 for wings 1, 2, and 3, respectively. (A design lift coefficient of 0 corresponds to a flat wing.) The remaining two wings had a 75° swept leading edge and an aspect ratio of 1.65. The design lift coefficients in this case are 0 and 0.16 for wings 4 and 5, respectively.

The all-steel wings were attached to a four-component strain-gage balance housed within the plate. The plate was supported in a horizontal position by the permanent sting mounting system of the Langley 4- by 4-foot supersonic pressure tunnel. During the tests, the wing and plate moved through an angle-of-attack range as a single unit. A clearance of 0.010 to 0.020 inch was provided between the wing root and the surface of the plate, except where the wing attaches to the balance.

The layout of the wing planforms and typical wing sections are shown in figure 2. Thickness distribution for all the wings was determined by a 3-percent-thick circular-arc airfoil section in the streamwise direction. This thickness was added symmetrically to the mean camber surface of the twisted and cambered wings. Ordinates of the mean camber surface based on the coordinate system shown in figure 3 are given in table I.

TESTS

The tests were conducted in the Langley 4- by 4-foot supersonic pressure tunnel with a free-stream Mach number of 2.05 and a Reynolds number of 4.4×10^6 based on the mean aerodynamic chord. In an effort to insure a turbulent boundary layer, transition strips were used on all wings. The strips, composed of a sparse distribution of No. 80 carborundum grains in a lacquer binder, were 1/8 of an inch wide and were located 1/4 inch behind the wing leading edges. Wings 1 and 5 were tested over a Reynolds number range of 1×10^6 to 4×10^6 to insure that the chosen test Reynolds number would be well above the transition regions.

The measurements of aerodynamic forces and moments were supplemented by a flow-visualization technique (ref. 10) which utilizes a fluorescent-oil film painted on the wing surface. The oil-flow pattern during tests can be used to indicate the direction of airflow at the wing surface and to indicate regions of detached flow.

Angle of attack was measured optically using prisms recessed in the wing surface.

From pretest calibrations and repeatability of the data, the Mach number and aerodynamic coefficients are estimated to be accurate within the following limits:

M	± 0.01
C_D	± 0.0003
C_L	± 0.0030
C_m	± 0.0010

DESIGN CONSIDERATIONS

In order to minimize transonic flow phenomena at the design conditions, wing-leading-edge sweep angles were chosen with consideration

given to the prevention of a sonic component of local flow perpendicular to the wing leading edge. The severe restriction this imposes can be seen in figure 4. Here the critical pressure coefficient corresponding to a sonic component of flow perpendicular to the leading edge of a swept wing has been plotted as a function of leading-edge sweep angle. The upper curve does not take into account the sidewash on the wing upper surface whereas the lower one does. The existence of this lower bound was not realized until after the wings were tested. Since these curves serve only as a guide and do not represent rigid requirements, it was felt that the chosen sweep angles of 70° and 75° would sufficiently minimize the possibility of transonic flow phenomena.

For a uniformly loaded wing it should be possible to reach lift coefficients equal to twice the critical pressure coefficient before encountering a transonic type of cross flow. In this case, a uniform load was not imposed on these wings so that the optimum loading might be more nearly approached. However, pressure coefficients in the vicinity of the leading edge were restricted to a value 1.4 times the average (or -0.7 times the design lift coefficient). The pressure coefficient of -0.112 that might be expected near the leading edge of wings designed for lift coefficient of 0.16 is shown in figure 4 for wings 3 and 5. Wing 2 was designed to produce a minimum drag at a lift coefficient of 0.08, and thus had only one-half the amount of camber as wing 3. At that lift coefficient the leading-edge pressure coefficient could be expected to be -0.056, which is below the critical, but additional lift must be generated by increased angle of attack before the maximum lift-drag ratio is reached. Thus each of the twisted and cambered wings would develop pressure coefficients near the critical value, but contrary to original expectations (as represented by the upper curve of fig. 4) none would be below. The addition of thickness to the mean camber surface produces an additional camber in the upper surface which has somewhat of a relieving effect on the pressures over the forward part of the wing.

The choice of the trailing-edge line was the result of a compromise between the desire for high aspect ratio and the need for structural rigidity. Similarly, the 3-percent-chord thickness of the circular-arc airfoil sections is believed to represent a reasonable compromise between low wave drag and structural considerations.

The camber surface was designed according to the methods of references 8 and 9. The loading distribution was obtained by a superposition of three types of loading combined in such a manner as to produce a minimum drag at a given design lift coefficient. The fundamental loadings considered were a uniform load, a linearly varying span load, and a linearly varying chord load. The resultant loading was subjected to the previously mentioned restriction that the leading-edge pressure coefficient not be greater than 1.4 times the average. The theoretical pressure

distribution at design condition may be expressed in the following manner:

For the upper surface

$$C_p = \frac{-C_{L,design}}{2}\left[1.4 + 1.846\left(\frac{y}{b/2} - \frac{x}{l}\right)\right]$$

and for the lower surface

$$C_p = \frac{C_{L,design}}{2}\left[1.4 + 1.846\left(\frac{y}{b/2} - \frac{x}{l}\right)\right]$$

The resultant theoretical lift-drag polars are as follows:

For the 70° swept wings

$$C_D = C_{D,o} + 0.230\left(C_{L,design}\right)^2 - 0.425\left(C_{L,design}\right)C_L + 0.500C_L{}^2$$

and for the 75° swept wings

$$C_D = C_{D,o} + 0.338\left(C_{L,design}\right)^2 - 0.633\left(C_{L,design}\right)C_L + 0.622C_L{}^2$$

RESULTS AND DISCUSSION

In order to evaluate the effectiveness of the transition strips in providing a fully turbulent boundary layer, two of the wings were tested over a Reynolds number range. Wings 1 and 5 were chosen for this purpose as being representative of a flat wing and a highly cambered one, respectively. In figure 5, the minimum drag coefficients are plotted against Reynolds number up to the test Reynolds number of 4.4×10^6. The variation of turbulent skin friction with Reynolds number according to Van Driest (ref. 11) has been computed. The estimated minimum drag coefficients shown in the figure were obtained by adding estimated wave drag and drag due to lift to the skin-friction values. For the flat wing, transition from laminar to turbulent flow appears to take place at a Reynolds number of about 2×10^6. The data for the twisted and cambered wing follow the turbulent line over the Reynolds number range. Thus, it

could be expected that turbulent flow would exist over all the wings at the test Reynolds number.

The aerodynamic characteristics in pitch of the five wings are given as a function of lift coefficient in figure 6. Data for wings of the same planform are plotted on a single set of axes for ease in making comparisons. In figure 6(a), note that the presence of twist and camber does not appreciably change the lift-curve slope.

As shown in figure 6(c), for the 70° swept wings, the wing designed for a lift coefficient of 0.16 produced a maximum lift-drag ratio of 8.3 whereas the wing designed for a lift coefficient of 0 produced a maximum lift-drag ratio of 8.1. This rather modest gain is overshadowed by the value for $(L/D)_{max}$ of 8.8 attained by the 70° swept wing employing the smaller amount of twist and camber corresponding to a design lift coefficient of 0.08. These data indicate that although there are sizable benefits to be derived from the use of wing warping, present design methods are not adequate to exploit this approach to the fullest possible extent. There is no reason to believe that the rather arbitrary choice of design lift coefficient for wing 2 has achieved the optimum loading. Similarly, for the 75° swept wings, the wing designed for a lift coefficient of 0.16 showed only a slightly higher maximum lift-drag ratio than did the flat wing - a value of 7.6 compared with 7.4.

L
8
7
6

A comparison of theoretical estimates with the measured data is presented in figure 7. The failure of all the wings to match the theoretical lift-curve slope may, in part, be due to the flow separation present in each case. Another factor is the aeroelastic deformation under load which tends to produce a loss of lift in the tip region. The sketches in figure 7 give an indication of the extent of separated flow on the wing surface. Observations and photographs of the fluorescent-oil film made during the tests were used in preparing the sketches. The photographs are not presented in this paper because they were of poor quality and would therefore not reproduce satisfactorily.

Note that for both flat wings (figs. 7(a) and 7(d)), separation occurred at the leading edge and, from its inception, occupied a large portion of the wing. On the other hand, for the twisted and cambered wings (figs. 7(b), 7(c), and 7(e)), separation appeared first at the inboard region along the trailing edge, and the area affected grew more steadily than that for the flat wings.

Linearized theory indicates a singularity at the leading edge of lifting flat-plate wings swept behind the Mach line. Actual upwash angularities just ahead of the leading edge are in all probability very high. The region of separated flow immediately behind the wing leading edge would appear to be caused by the inability of the real flow to negotiate

the sharp turns necessary for attachment. When the flow above the separated region does return to the wing surface, it is redirected along the wing surface and results in a recompression and a shock. This is the type of separation experienced by the flat wings. The twisted and cambered wings were designed to eliminate the singularity at design lift coefficient and thus might be expected to avoid leading-edge separation, at least near design conditions. The test data indicate that leading-edge separation of the turbulent boundary layer did not occur on the twisted and cambered wing within the angle-of-attack range used here.

At the trailing edge of a wing at an angle of attack, the flow along the wing surface is redirected in a nearly streamwise direction causing a recompression and a trailing-edge shock. If the pressure rise across the shock is too strong, a turbulent boundary layer cannot pass through the shock without separating. In that case the flow would leave the surface just enough to reduce the flow angle and shock strength to the critical value. From considerations of two-dimensional boundary layers, it would appear that the pressure rise at the trailing edge predicted for these wings would not cause separation. Nevertheless, flow separation in the vicinity of the trailing edge of each of the twisted and cambered wings is evident from oil-flow observations. Of course, there is quite a departure from two-dimensional flow in this case. In addition, although local flow in the free-stream direction is assumed in making the calculations, there actually is a considerable sidewash which in the case of the twisted and cambered wings results in greater surface slopes and higher negative pressures at the trailing edge than those given by the theory.

From the oil-flow observations there was no evidence of local shocks or transonic flow phenomena near the leading edge of any of the twisted and cambered wings. Thus it appears that the restrictions on leading-edge sweep angle and loading at the leading edge produced the desired result of avoiding these effects.

In spite of the loss in lift, both flat wings (figs. 7(a) and 7(d)) showed a lift-drag polar in close agreement with the theory. This agreement may result from the presence of some degree of leading-edge suction or, perhaps, may result from an improved loading distribution brought about by aeroelastic twist. Although each of the twisted and cambered wings (figs. 7(b), 7(c), and 7(e)) showed some improvement in maximum lift-drag ratio over that obtained for the flat wings as previously noted, they fail by a considerable margin to match the theory. A part of this failure may be due to the separated flow. However, it may also be due to the inability of linearized theory to provide a camber surface with the proper matching of pressures and surface slopes.

It is possible that wings designed for optimum loadings at lift coefficients somewhat below optimum may achieve a substantial amount of the

theoretical leading-edge suction at optimum lift coefficient. It may, in part, be this factor which allows the wing designed for a lift coefficient of 0.08 to have a higher value of $(L/D)_{max}$ than that for the wing designed for a lift coefficient of 0.16.

An interesting analysis can be made by comparing experimental axial force with the theoretical value for the cases of no leading-edge suction and full leading-edge suction. In figure 8, axial-force coefficient has been plotted as a function of lift coefficient for all the wings. Note that for regions on each side of the design lift coefficient, the experimental data generally follow the trend of the theoretical curve for the case of full leading-edge suction. At high lift coefficients, only a small portion of the predicted thrust force or leading-edge suction is realized. The increase in the axial-force level for the severely twisted and cambered wings may be the result of the failure of linearized theory to match properly pressures and surface slopes under these conditions.

The variation with design lift coefficient (degree of twisted camber) of the maximum lift-drag ratio and the corresponding lift coefficient is shown in figure 9. The optimum lift coefficients agree well with the theoretical curve for the case of no leading-edge suction. For this series of wings, the amount of twist and camber that can profitably be used in developing high lift-drag ratios corresponds to a design lift coefficient well below the lift coefficient for $(L/D)_{max}$. The design lift coefficient of 0.08 may well be near the optimum for this family. Note that the value for $(L/D)_{max}$ of 8.8 found for that wing, although considerably above the value of 8.1 for the flat 70° swept wing, is still far below the theoretical maximum value of 10.2. (See fig. 9(a).)

As the design lift coefficient is increased, the amount of leading-edge suction theoretically available is reduced, but the possibility of achieving any large percentage of that available may be increased. Another consequence of high design lift coefficients is the increase in drag which may result from the inability of linearized theory to match properly local pressures and surface slopes when extreme camber and strong disturbances are present. Camber also influences the type and degree of flow separation. All these factors, and perhaps more, make the task of finding an optimum twist and camber distribution very difficult.

CONCLUSIONS

An experimental investigation at a Mach number of 2.05 of several twisted and cambered arrow wings and the corresponding flat wings provides the following conclusions:

1. A 70° swept arrow wing with twist and camber designed for an optimum loading at a lift coefficient considerably less than that for maximum lift-drag ratio gave the highest lift-drag ratio of all the wings tested - a value of 8.8 compared with a value of 8.1 for the corresponding wing without twist and camber.

2. Two twisted and cambered wings designed for optimum loading at the lift coefficient for maximum lift-drag ratio gave only small increases in maximum lift-drag ratio over that obtained for the corresponding flat wings.

3. In all cases, the lift-drag ratios obtained were far below the theoretical estimates.

4. Proper selection of loading at the leading edge and of leading-edge sweep angles for the twisted and cambered wings produced the desired result of avoiding leading-edge separation and transonic flow phenomena near the leading edge. However, regions of separated flow in the vicinity of the trailing edge were present on each of the twisted and cambered wings.

Langley Research Center,
National Aeronautics and Space Administration,
Langley Field, Va., June 22, 1960.

REFERENCES

1. Jones, Robert T.: Estimated Lift-Drag Ratios at Supersonic Speed. NACA TN 1350, 1947.

2. Brown, Clinton E., and McLean, Francis E.: The Problem of Obtaining High Lift-Drag Ratios at Supersonic Speeds. Jour. Aero/Space Sci., vol. 26, no. 5, May 1959, pp. 298-302.

3. Jones, Robert T.: The Minimum Drag of Thin Wings in Frictionless Flow. Jour. Aero. Sci., vol. 18, no. 2, Feb. 1951, pp. 75-81.

4. Jones, Robert T.: Theoretical Determination of the Minimum Drag of Airfoils at Supersonic Speeds. Jour. Aero. Sci., vol. 19, no. 12, Dec. 1952, pp. 813-822.

5. Madden, Robert T.: Aerodynamic Study of a Wing-Fuselage Combination Employing a Wing Swept Back 63° - Investigation at a Mach Number of 1.53 To Determine the Effects of Cambering and Twisting the Wing for Uniform Load at a Lift Coefficient of 0.25. NACA RM A9C07, 1949.

6. Brown, Clinton E., and Hargrave, L. K.: Investigation of Minimum Drag and Maximum Lift-Drag Ratios of Several Wing-Body Combinations Including a Cambered Triangular Wing at Low Reynolds Numbers and at Supersonic Speeds. NACA TN 4020, 1958. (Supersedes NACA RM L51E11.)

7. Hallissy, Joseph M., Jr., and Hasson, Dennis F.: Aerodynamic Characteristics at Mach Numbers 2.36 and 2.87 of an Airplane Configuration Having a Cambered Arrow Wing With a 75° Swept Leading Edge. NACA RM L58E21, 1958.

8. Tucker, Warren A.: A Method for the Design of Sweptback Wings Warped To Produce Specified Flight Characteristics at Supersonic Speeds. NACA Rep. 1226, 1955. (Supersedes NACA RM L51F08.)

9. Grant, Frederick C.: The Proper Combination of Lift Loadings for Least Drag on a Supersonic Wing. NACA Rep. 1275, 1956. (Supersedes NACA TN 3533.)

10. Loving, Donald L., and Katzoff, S.: The Fluorescent-Oil Film Method and Other Techniques for Boundary-Layer Flow Visualization. NASA MEMO 3-17-59L, 1959.

11. Van Driest, E. R.: Turbulent Boundary Layer in Compressible Fluids. Jour. Aero. Sci., vol. 18, no. 3, Mar. 1951, pp. 145-160, 216.

TABLE I

CAMBER-SURFACE ORDINATES

(a) Wing 2. $\Lambda = 70^{\circ}$; $C_{L,design} = 0.08$

$\frac{y'}{b'}$	Camber-surface ordinate z/l at -										
	$\frac{x'}{c'} = 0$	$\frac{x'}{c'} = 0.05$	$\frac{x'}{c'} = 0.10$	$\frac{x'}{c'} = 0.15$	$\frac{x'}{c'} = 0.20$	$\frac{x'}{c'} = 0.25$	$\frac{x'}{c'} = 0.30$	$\frac{x'}{c'} = 0.35$	$\frac{x'}{c'} = 0.40$	$\frac{x'}{c'} = 0.45$	$\frac{x'}{c'} = 0.50$
0	0.0320	------	------	------	------	------	------	------	------	------	------
.05	.0209	------	------	------	0.0231	------	------	------	0.0249	------	------
.10	.0125	------	0.0143	------	.0157	------	0.170	------	.0182	------	0.0194
.15	.0077	0.0087	.0094	0.0100	.0106	0.0111	.0117	0.0123	.0130	0.0134	.0140
.20	.0043	.0053	.0061	.0067	.0074	.0078	.0082	.0085	.0089	.0094	.0097
.25	.0023	.0034	.0040	.0044	.0049	.0053	.0055	.0058	.0060	.0062	.0062
.30	.0015	.0023	.0028	.0030	.0031	.0032	.0033	.0034	.0034	.0033	.0033
.35	.0016	.0023	.0024	.0023	.0022	.0021	.0019	.0016	.0013	.0011	.0010
.40	.0018	.0026	.0028	.0026	.0020	.0014	.0008	.0003	-.0003	-.0007	-.0012
.45	.0020	.0030	.0033	.0028	.0022	.0015	.0006	-.0005	-.0013	-.0022	-.0031
.50	.0023	.0034	.0034	.0030	.0024	.0016	.0005	-.0008	-.0023	-.0035	-.0047
.55	.0025	.0036	.0037	.0034	.0028	.0018	.0007	-.0006	-.0022	-.0039	-.0055
.60	.0027	.0037	.0039	.0037	.0034	.0029	.0021	.0011	-.0000	-.0013	-.0027
.65	.0029	.0038	.0042	.0042	.0040	.0036	.0031	.0024	.0017	.0008	-.0002
.70	.0031	.0040	.0044	.0045	.0044	.0041	.0039	.0034	.0030	.0025	.0018
.75	.0033	.0042	.0046	.0048	.0048	.0047	.0045	.0043	.0040	.0036	.0032
.80	.0035	.0042	.0047	.0050	.0051	.0051	.0051	.0050	.0049	.0047	.0044
.85	.0037	.0043	.0047	.0051	.0053	.0054	.0054	.0054	.0054	.0053	.0053
.90	.0039	------	.0046	------	.0052	------	.0054	------	.0056	------	.0057
.95	.0041	------	------	------	.0048	------	------	------	.0054	------	------
1.00	.0043	------	------	------	------	------	------	------	------	------	------

$\frac{y'}{b'}$	Camber-surface ordinate z/l at -										
	$\frac{x'}{c'} = 0.55$	$\frac{x'}{c'} = 0.60$	$\frac{x'}{c'} = 0.65$	$\frac{x'}{c'} = 0.70$	$\frac{x'}{c'} = 0.75$	$\frac{x'}{c'} = 0.80$	$\frac{x'}{c'} = 0.85$	$\frac{x'}{c'} = 0.90$	$\frac{x'}{c'} = 0.95$	$\frac{x'}{c'} = 1.00$
0.05	------	0.0260	------	------	------	0.0269	------	------	------	0.0273
.10	------	------	0.0203	------	0.0211	------	0.0218	------	0.0223	.0226
.15	0.0146	.0150	.0155	0.0159	.0163	.0166	.0169	0.0171	.0174	.0177
.20	.0101	.0105	.0108	.0112	.0115	.0118	.0120	.0122	.0124	.0125
.25	.0064	.0065	.0067	.0069	.0070	.0070	.0071	.0072	.0072	.0072
.30	.0032	.0030	.0030	.0029	.0026	.0025	.0023	.0022	.0020	.0017
.35	.0007	.0002	-.0003	-.0009	-.0015	-.0018	-.0022	-.0025	-.0033	-.0042
.40	-.0019	-.0024	-.0031	-.0039	-.0048	-.0055	-.0063	-.0070	-.0084	-.0101
.45	-.0039	-.0048	-.0057	-.0067	-.0078	-.0090	-.0104	-.0115	-.0134	-.0162
.50	-.0058	-.0070	-.0081	-.0093	-.0108	-.0126	-.0145	-.0161	-.0185	-.0224
.55	-.0071	-.0086	-.0098	-.0111	-.0127	-.0142	-.0161	-.0182	-.0208	-.0249
.60	-.0043	-.0059	-.0076	-.0090	-.0105	-.0117	-.0131	-.0143	-.0157	-.0173
.65	-.0014	-.0025	-.0038	-.0051	-.0067	-.0082	-.0097	-.0110	-.0124	-.0137
.70	.0011	.0003	-.0006	-.0015	-.0026	-.0037	-.0048	-.0060	-.0072	-.0085
.75	.0028	.0022	.0016	.0010	.0003	-.0003	-.0010	-.0018	-.0027	-.0036
.80	.0042	.0038	.0035	.0032	.0028	.0023	.0018	.0014	.0008	.0003
.85	.0052	.0050	.0049	.0047	.0045	.0043	.0041	.0038	.0036	.0033
.90	------	.0056	------	.0055	------	.0054	------	.0053	------	.0051
.95	------	.0057	------	------	------	.0058	------	------	------	.0059

TABLE I.- Continued

CAMBER-SURFACE ORDINATES

(b) Wing 3. $\Lambda = 70^{\circ}$; $C_{L,design} = 0.16$

$\frac{y'}{b'}$	Camber-surface ordinate z/l at -										
	$\frac{x'}{c'} = 0$	$\frac{x'}{c'} = 0.05$	$\frac{x'}{c'} = 0.10$	$\frac{x'}{c'} = 0.15$	$\frac{x'}{c'} = 0.20$	$\frac{x'}{c'} = 0.25$	$\frac{x'}{c'} = 0.30$	$\frac{x'}{c'} = 0.35$	$\frac{x'}{c'} = 0.40$	$\frac{x'}{c'} = 0.45$	$\frac{x'}{c'} = 0.50$
0	0.0640	------	------	------	------	------	------	------	------	------	------
.05	.0417	------	------	------	0.0462	------	------	------	0.0496	------	------
.10	.0251	------	0.0286	------	.0314	------	0.0340	------	.0026	------	0.0389
.15	.0155	0.0174	.0189	0.0200	.0212	0.0223	.0234	0.0246	.0259	0.0269	.0281
.20	.0087	.0106	.0122	.0135	.0147	.0156	.0164	.0171	.0179	.0187	.0193
.25	.0046	.0067	.0080	.0089	.0098	.0106	.0110	.0116	.0120	.0124	.0125
.30	.0031	.0047	.0054	.0060	.0062	.0064	.0065	.0068	.0067	.0068	.0066
.35	.0032	.0046	.0048	.0047	.0044	.0042	.0037	.0031	.0026	.0023	.0019
.40	.0037	.0053	.0057	.0051	.0040	.0028	.0017	.0005	-.0006	-.0014	-.0025
.45	.0041	.0059	.0061	.0056	.0044	.0029	.0011	-.0009	-.0026	-.0045	-.0062
.50	.0045	.0067	.0068	.0061	.0049	.0031	.0010	-.0016	-.0046	-.0070	-.0094
.55	.0050	.0072	.0074	.0067	.0055	.0036	.0014	-.0013	-.0043	-.0077	-.0109
.60	.0054	.0073	.0078	.0076	.0069	.0057	.0042	.0022	-.0001	-.0026	-.0054
.65	.0058	.0076	.0084	.0085	.0081	.0072	.0061	.0048	.0033	.0015	-.0005
.70	.0062	.0080	.0088	.0090	.0087	.0083	.0077	.0069	.0059	.0049	.0036
.75	.0066	.0083	.0091	.0096	.0096	.0094	.0091	.0086	.0080	.0072	.0064
.80	.0070	.0085	.0094	.0099	.0102	.0102	.0102	.0100	.0098	.0094	.0089
.85	.0074	.0086	.0095	.0102	.0106	.0108	.0109	.0109	.0108	.0107	.0106
.90	.0078	------	.0092	------	.0103	------	.0109	------	.0112	------	.0114
.95	.0082	------	------	------	.0097	------	------	------	.0107	------	------
1.00	.0085	------	------	------	------	------	------	------	------	------	------

$\frac{y'}{b'}$	Camber-surface ordinate z/l at -									
	$\frac{x'}{c'} = 0.55$	$\frac{x'}{c'} = 0.60$	$\frac{x'}{c'} = 0.65$	$\frac{x'}{c'} = 0.70$	$\frac{x'}{c'} = 0.75$	$\frac{x'}{c'} = 0.80$	$\frac{x'}{c'} = 0.85$	$\frac{x'}{c'} = 0.90$	$\frac{x'}{c'} = 0.95$	$\frac{x'}{c'} = 1.00$
0.05	------	0.0520	------	------	------	0.0541	------	------	------	0.0546
.10	------	.0407	------	0.0422	------	.0435	------	0.0445	------	.0453
.15	0.0293	.0301	0.0310	.0318	0.0326	.0333	0.0338	.0343	0.0349	.0354
.20	.0203	.0210	.0217	.0225	.0230	.0237	.0240	.0243	.0248	.0251
.25	.0128	.0130	.0134	.0136	.0139	.0141	.0142	.0143	.0144	.0144
.30	.0064	.0061	.0059	.0058	.0053	.0050	.0046	.0045	.0040	.0034
.35	.0014	.0005	-.0005	-.0018	-.0029	-.0037	-.0043	-.0051	-.0066	-.0083
.40	-.0037	-.0047	-.0062	-.0079	-.0096	-.0110	-.0125	-.0140	-.0168	-.0202
.45	-.0078	-.0096	-.0076	-.0133	-.0155	-.0181	-.0206	-.0230	-.0269	-.0324
.50	-.0117	-.0139	-.0162	-.0186	-.0216	-.0251	-.0290	-.0323	-.0371	-.0448
.55	-.0142	-.0171	-.0197	-.0222	-.0254	-.0285	-.0322	-.0365	-.0416	-.0497
.60	-.0086	-.0118	-.0152	-.0181	-.0210	-.0237	-.0262	-.0286	-.0315	-.0345
.65	-.0027	-.0050	-.0075	-.0102	-.0134	-.0165	-.0193	-.0221	-.0248	-.0275
.70	.0021	.0006	-.0011	-.0030	-.0051	-.0073	-.0096	-.0120	-.0144	-.0169
.75	.0055	.0043	.0032	.0019	.0006	-.0006	-.0021	-.0036	-.0054	-.0072
.80	.0083	.0077	.0070	.0063	.0055	.0046	.0037	.0027	.0016	.0006
.85	.0104	.0101	.0098	.0093	.0090	.0086	.0082	.0076	.0071	.0065
.90	.0101	.0113	------	.0110	------	.0108	------	.0105	------	------
.95	------	.0113	------	------	------	.0117	------	------	------	.0119

TABLE I.- Concluded

CAMBER-SURFACE ORDINATES

(c) Wing 5. $\Lambda = 75^{\circ}$; $C_{L,design} = 0.16$

$\frac{y'}{b'}$	Camber-surface ordinate z/l at -										
	$\frac{x'}{c'} = 0$	$\frac{x'}{c'} = 0.05$	$\frac{x'}{c'} = 0.10$	$\frac{x'}{c'} = 0.15$	$\frac{x'}{c'} = 0.20$	$\frac{x'}{c'} = 0.25$	$\frac{x'}{c'} = 0.30$	$\frac{x'}{c'} = 0.35$	$\frac{x'}{c'} = 0.40$	$\frac{x'}{c'} = 0.45$	$\frac{x'}{c'} = 0.50$
0.00	0.0789	------	------	------	------	------	------	------	------	------	------
.05	.0542	------	------	------	0.0596	------	------	------	0.0636	------	------
.10	.0345	------	0.0387	------	.0424	------	0.0462	------	.0491	------	0.0518
.15	.0209	------	.0264	------	.0305	------	.0338	------	.0368	------	.0397
.20	.0129	0.0159	.0180	0.0196	.0212	0.0227	.0243	0.0258	.0273	0.0286	.0299
.25	.0081	.0107	.0126	.0142	.0155	.0167	.0177	.0188	.0197	.0206	.0216
.30	.0062	.0086	.0100	.0109	.0118	.0126	.0131	.0136	.0139	.0143	.0146
.35	.0072	.0098	.0104	.0106	.0105	.0102	.0099	.0095	.0091	.0086	.0080
.40	.0081	.0106	.0115	.0113	.0105	.0092	.0077	.0065	.0054	.0043	.0032
.45	.0091	.0123	.0131	.0129	.0118	.0102	.0078	.0051	.0030	.0010	-.0010
.50	.0099	.0131	.0140	.0138	.0126	.0107	.0083	.0052	.0019	-.0011	-.0042
.55	.0110	.0144	.0153	.0149	.0136	.0115	.0088	.0054	.0016	-.0027	-.0069
.60	.0120	.0157	.0168	.0163	.0151	.0131	.0105	.0072	.0032	-.0013	-.0061
.65	.0128	.0163	.0176	.0176	.0170	.0157	.0141	.0120	.0095	.0067	.0032
.70	.0137	.0170	.0184	.0189	.0187	.0182	.0172	.0157	.0139	.0118	.0093
.75	.0147	.0171	.0185	.0192	.0195	.0194	.0192	.0185	.0176	.0163	.0149
.80	.0155	.0180	.0195	.0204	.0210	.0211	.0211	.0208	.0204	.0198	.0190
.85	.0163	.0182	.0196	.0205	.0211	.0216	.0220	.0221	.0221	.0221	.0218
.90	.0171	------	.0195	------	.0210	------	.0219	------	.0225	------	.0229
.95	.0179	------	------	------	.0206	------	------	------	.0222	------	------
1.00	.0187	------	------	------	------	------	------	------	------	------	------

$\frac{y'}{b'}$	Camber-surface ordinate z/l at -										
	$\frac{x'}{c'} = 0.55$	$\frac{x'}{c'} = 0.60$	$\frac{x'}{c'} = 0.65$	$\frac{x'}{c'} = 0.70$	$\frac{x'}{c'} = 0.75$	$\frac{x'}{c'} = 0.80$	$\frac{x'}{c'} = 0.85$	$\frac{x'}{c'} = 0.90$	$\frac{x'}{c'} = 0.95$	$\frac{x'}{c'} = 1.00$
0.05	------	0.0664	------	------	------	0.0683	------	------	------	0.0693
.10	------	.0539	------	0.0556	------	.0570	------	0.0582	------	.0590
.15	------	.0423	------	.0446	------	.0465	------	.0480	------	.0489
.20	0.0312	.0323	0.0333	.0343	0.0352	.0360	0.0367	.0373	0.0376	.0378
.25	.0224	.0231	.0239	.0246	.0251	.0256	.0259	.0261	.0263	.0264
.30	.0149	.0150	.0152	.0153	.0154	.0154	.0153	.0150	.0147	.0144
.35	.0076	.0070	.0067	.0062	.0057	.0050	.0042	.0034	.0024	.0043
.40	.0019	.0008	-.0005	-.0016	-.0030	-.0045	-.0060	-.0077	-.0096	-.0117
.45	-.0029	-.0048	-.0067	-.0088	-.0110	-.0133	-.0157	-.0184	-.0216	-.0256
.50	-.0071	-.0101	-.0129	-.0155	-.0184	-.0213	-.0245	-.0283	-.0337	-.0402
.55	-.0105	-.0139	-.0178	-.0217	-.0249	-.0283	-.0325	-.0387	-.0458	-.0558
.60	-.0114	-.0161	-.0205	-.0245	-.0282	-.0320	-.0360	-.0408	-.0466	-.0560
.65	-.0008	-.0050	-.0096	-.0146	-.0193	-.0235	-.0274	-.0314	-.0350	-.0389
.70	.0068	.0040	.0011	-.0022	-.0056	-.0094	-.0134	-.0177	-.0220	-.0265
.75	.0132	.0115	.0096	.0074	.0050	.0025	-.0003	-.0032	-.0061	-.0093
.80	.0182	.0172	.0161	.0149	.0136	.0122	.0104	.0085	.0067	.0049
.85	.0216	.0211	.0206	.0200	.0194	.0187	.0179	.0170	.0162	.0152
.90	.0217	.0229	------	.0229	------	.0227	------	.0223	------	------
.95	------	.0232	------	------	------	.0238	------	------	------	0.0241

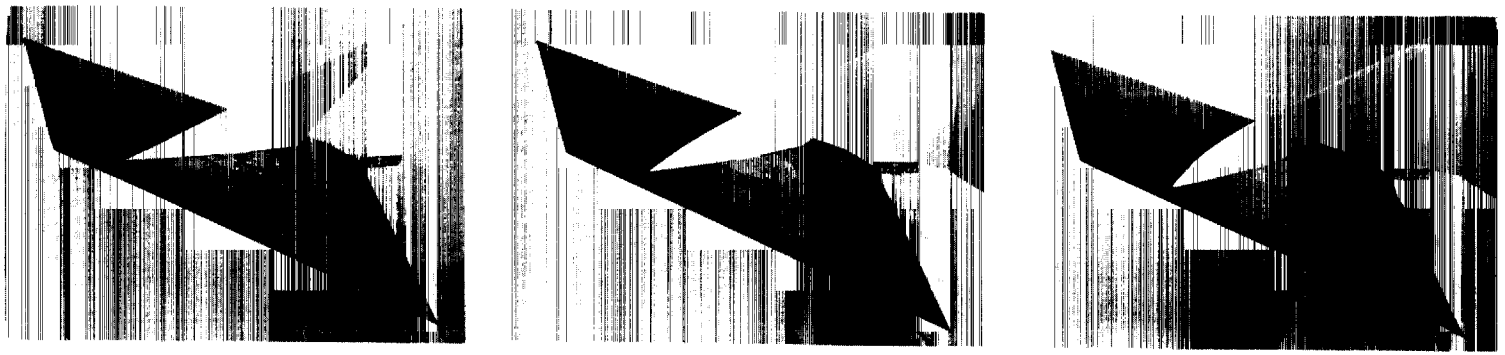

(a) Wing 1. $\Lambda = 70^{\circ}$; $C_{L,design} = 0$.

(b) Wing 2. $\Lambda = 70^{\circ}$; $C_{L,design} = 0.08$.

(c) Wing 3. $\Lambda = 70^{\circ}$; $C_{L,design} = 0.16$.

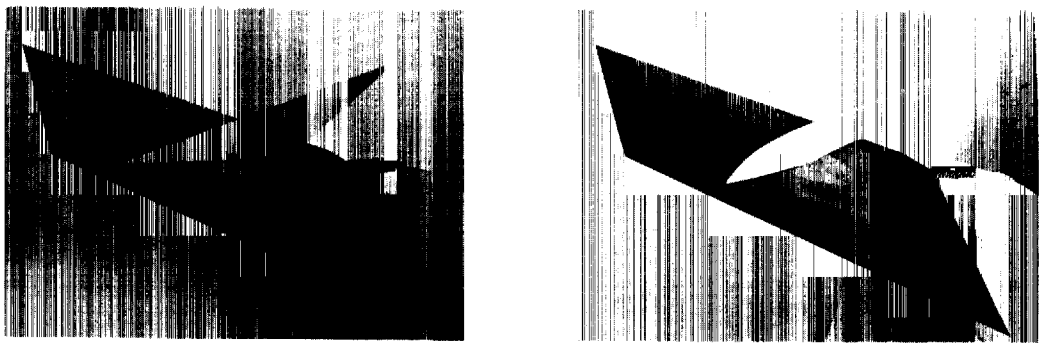

(d) Wing 4. $\Lambda = 75^{\circ}$; $C_{L,design} = 0$.

(e) Wing 5. $\Lambda = 75^{\circ}$; $C_{L,design} = 0.16$.

L-60-2494

Figure 1.- Photographs of the models mounted on the boundary-layer bypass plate.

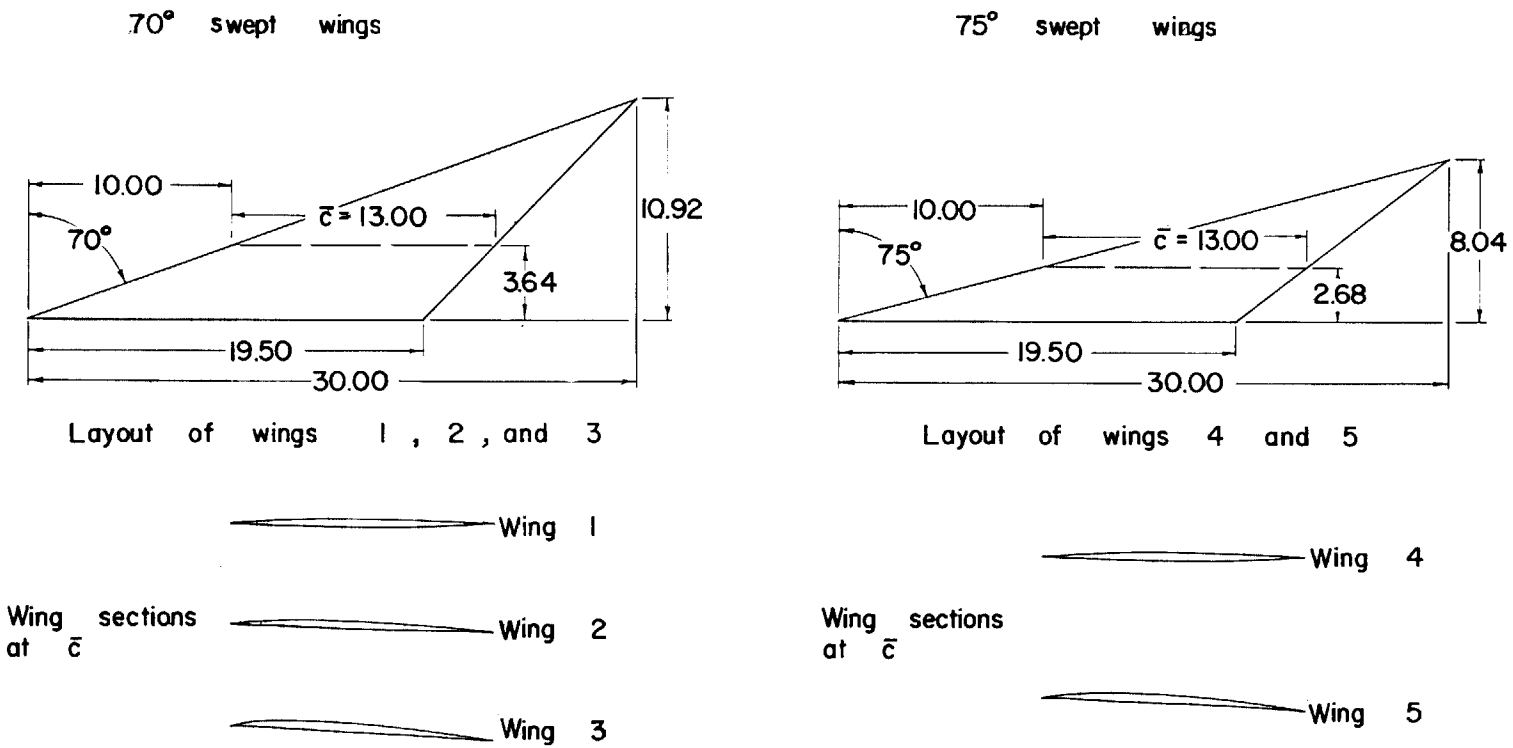

Figure 2.- Planforms and typical sections of the series of wings. All wings employ a 3-percent-thick circular-arc streamwise airfoil section. All dimensions are in inches.

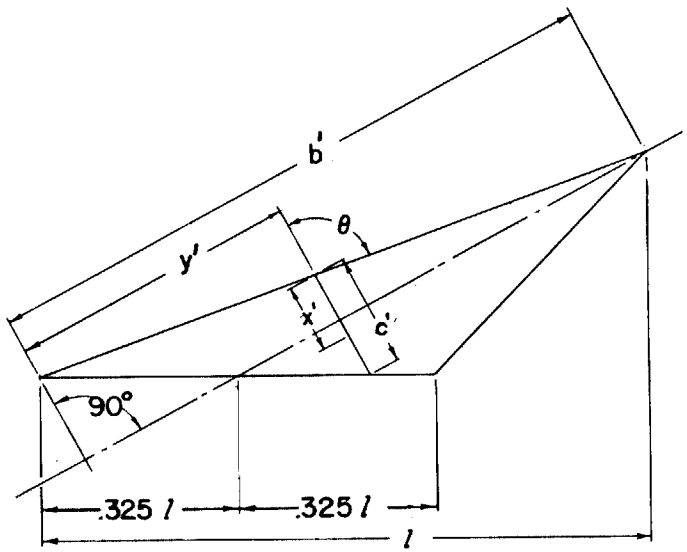

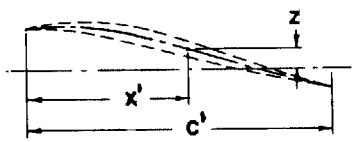

70° Swept Wing $\theta = 98.334°$	
y'/b'	c'/l
0	0
.05	.02068
.10	.04135
.15	.06203
.20	.08270
.25	.10338
.30	.12405
.35	.14473
.40	.16540
.45	.18608
.50	.20676
.55	.22142
.60	.19682
.65	.17221
.70	.14761
.75	.12301
.80	.09841
.85	.07381
.90	.04920
.95	.02460
1.00	0

75° Swept Wing $\theta = 96.651°$	
y'/b'	c'/l
0	0
.05	.01441
.10	.02883
.15	.04324
.20	.05756
.25	.07207
.30	.08649
.35	.10090
.40	.11531
.45	.12973
.50	.14414
.55	.15856
.60	.16425
.65	.14371
.70	.12318
.75	.10265
.80	.08212
.85	.06159
.90	.04106
.95	.02053
1.00	0

Figure 3.- Coordinate system used in describing the camber surface. Refer to table I.

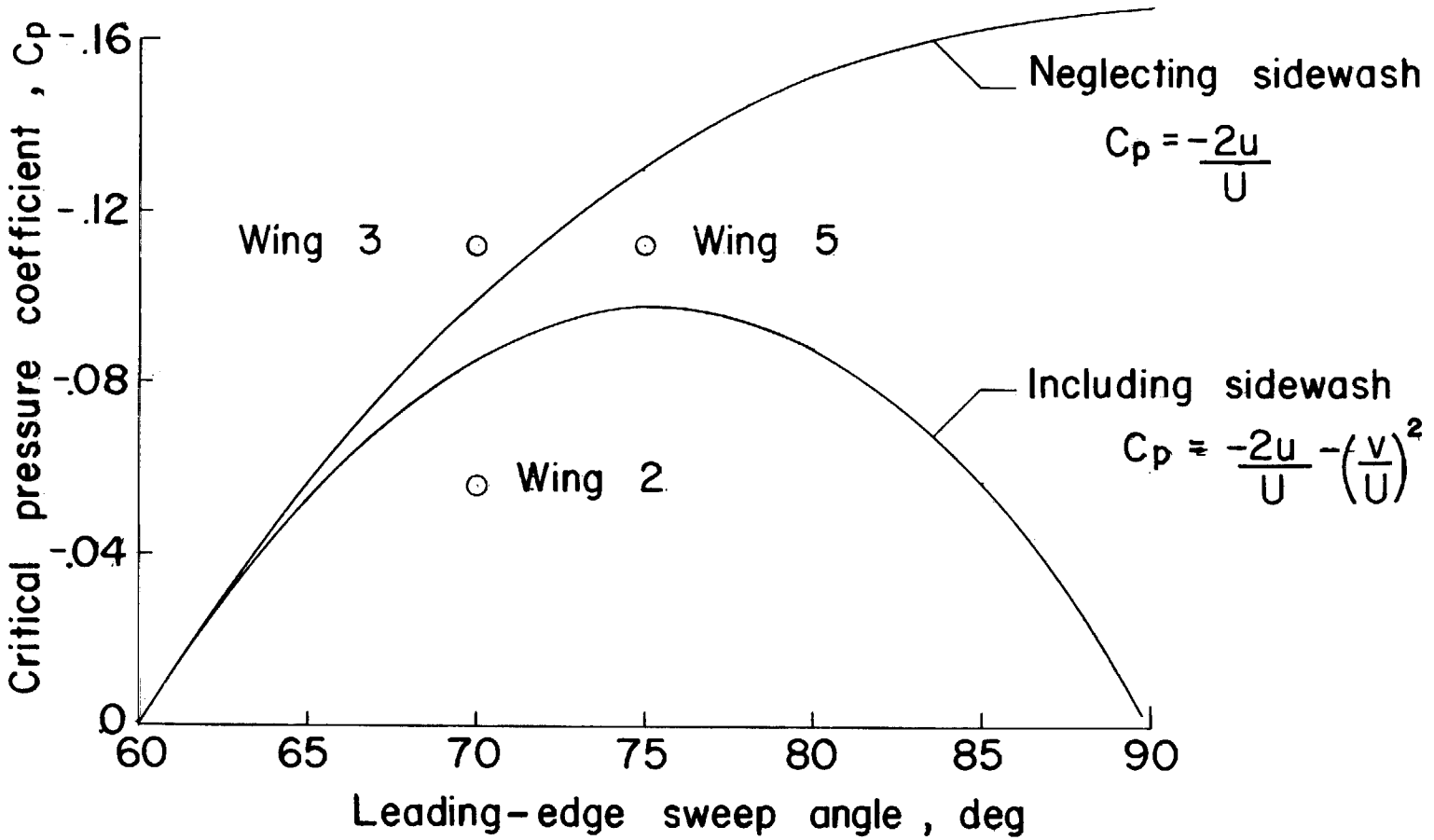

Figure 4.- Pressure coefficient corresponding to a sonic speed component of flow perpendicular to the wing leading edge as a function of sweep angle. M = 2. Symbols give the theoretical pressure at the leading edge of the twisted and cambered wings for the design lift coefficient.

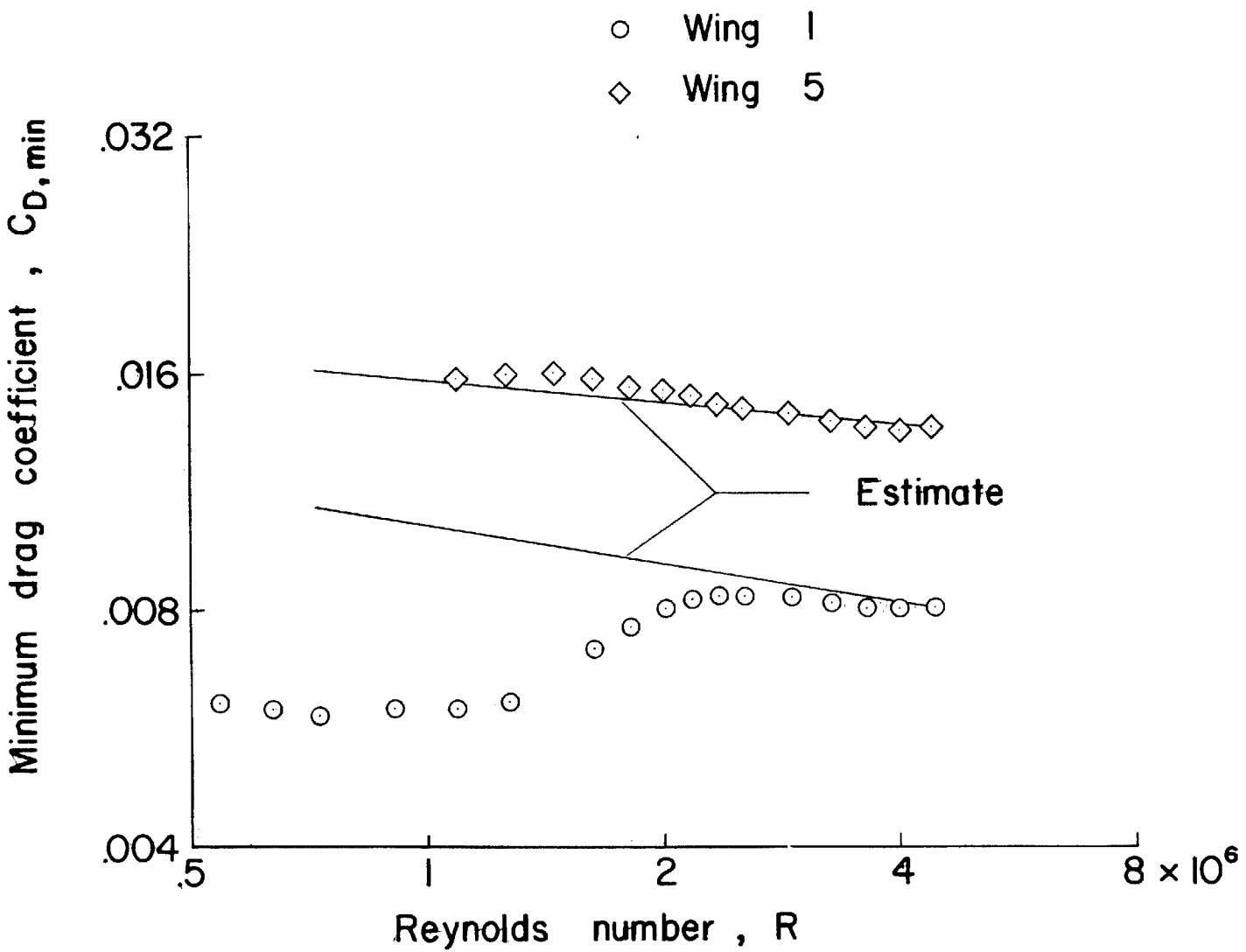

Figure 5.- Variation of minimum drag coefficient with Reynolds number.

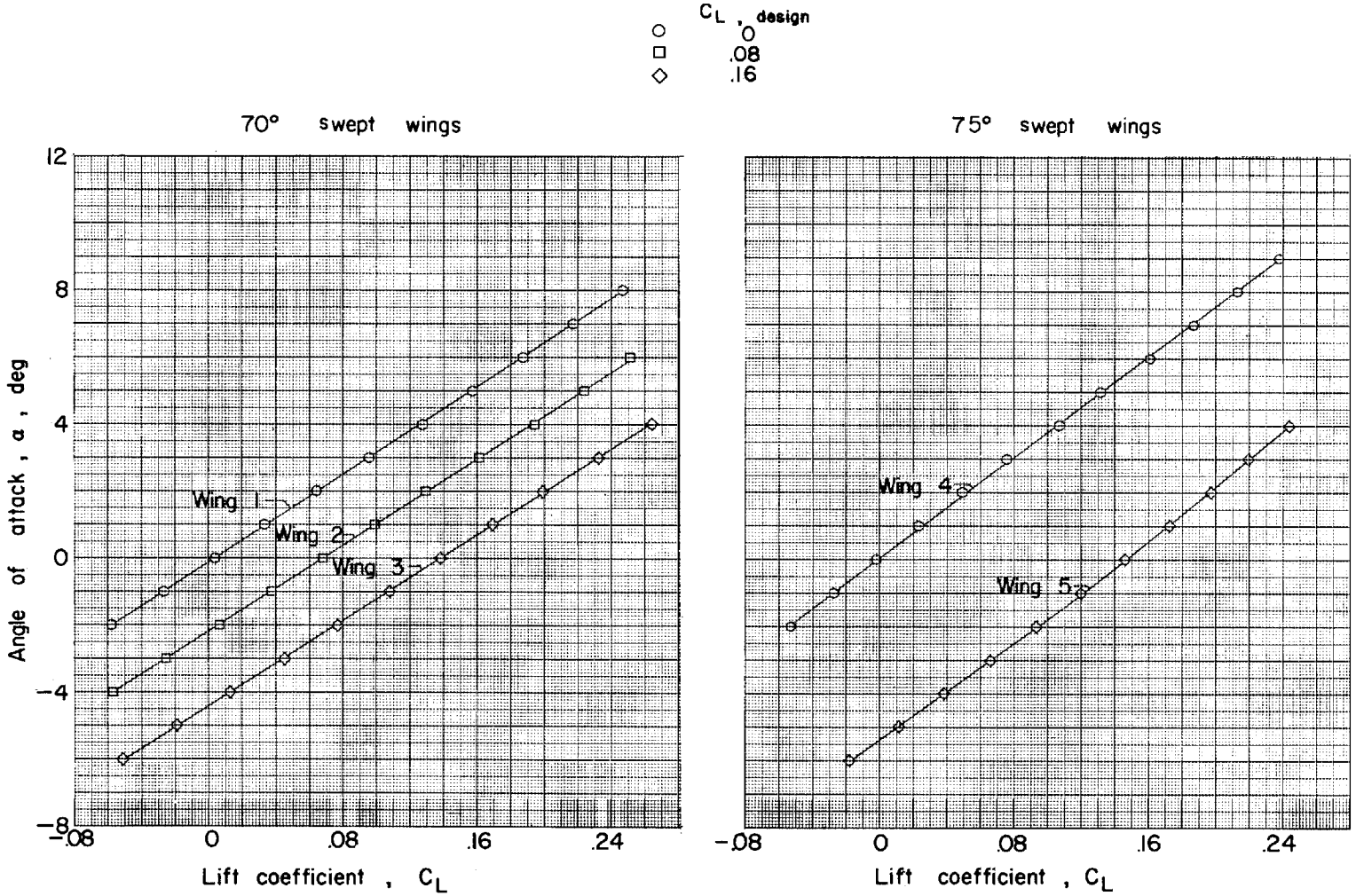

(a) Angle of attack as a function of lift coefficient.

Figure 6.- Measured aerodynamic characteristics in pitch.

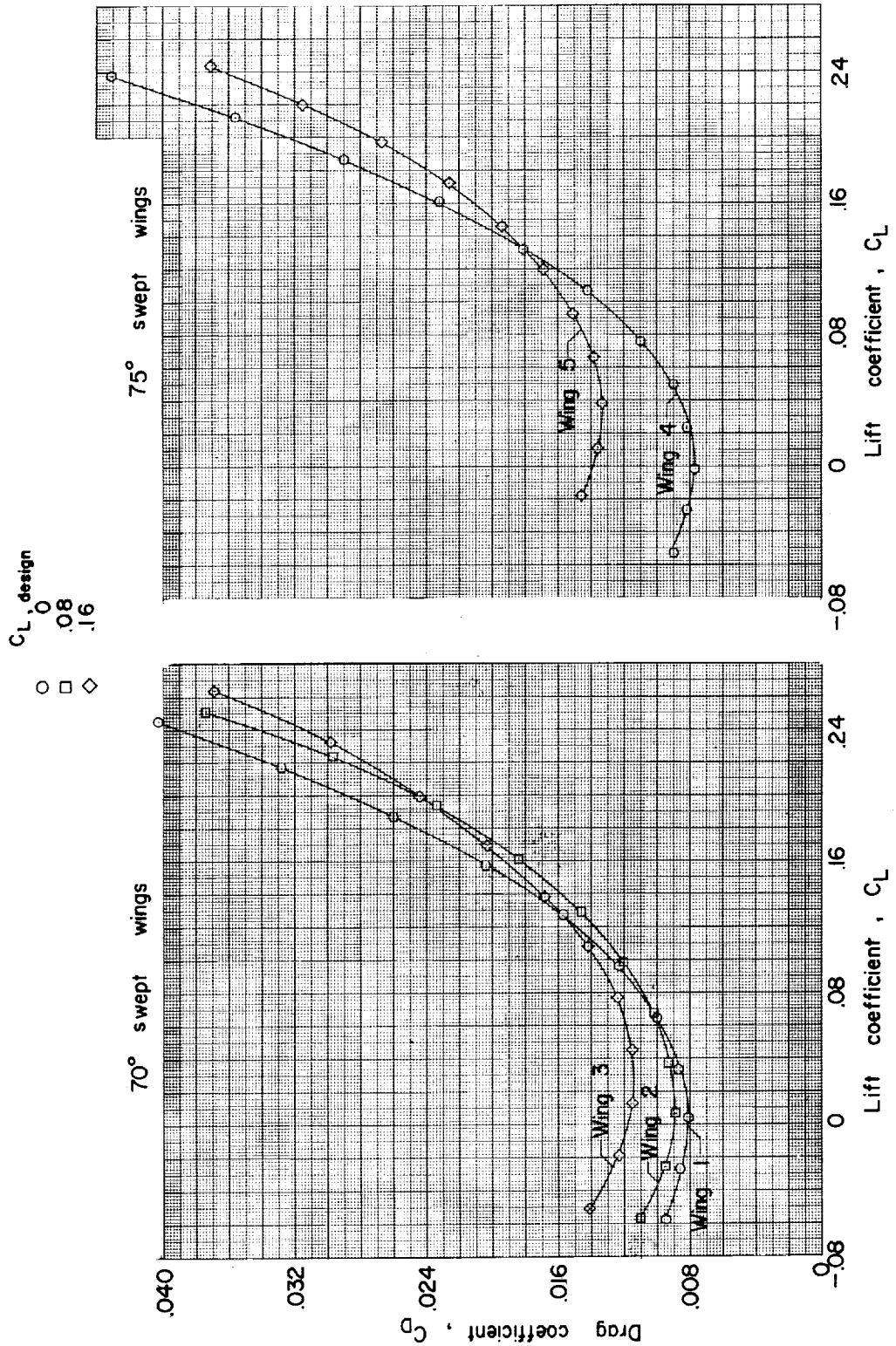

(b) Drag coefficient as a function of lift coefficient.

Figure 6.- Continued.

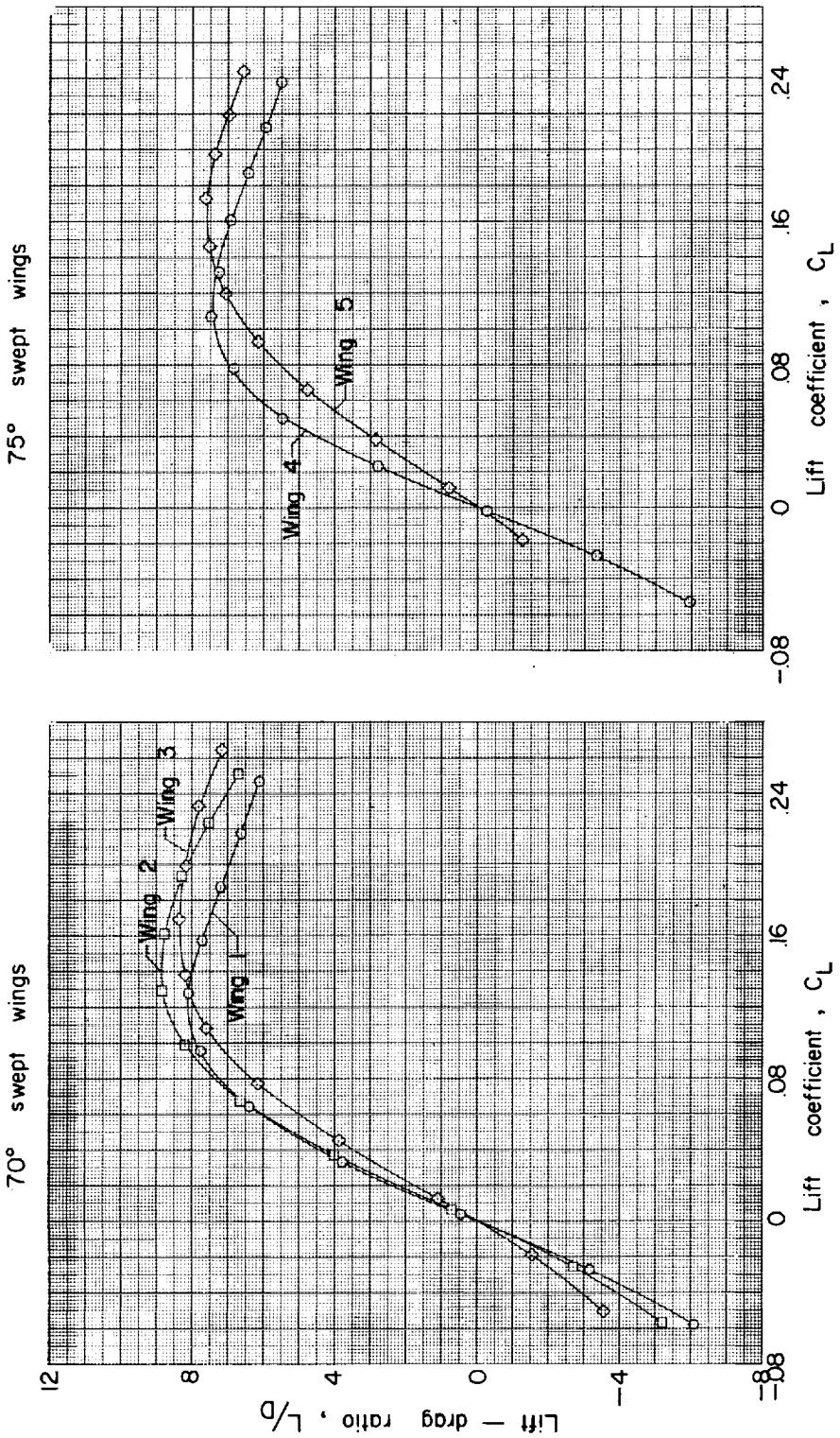

(c) Lift-drag ratio as a function of lift coefficient.

Figure 6.- Continued.

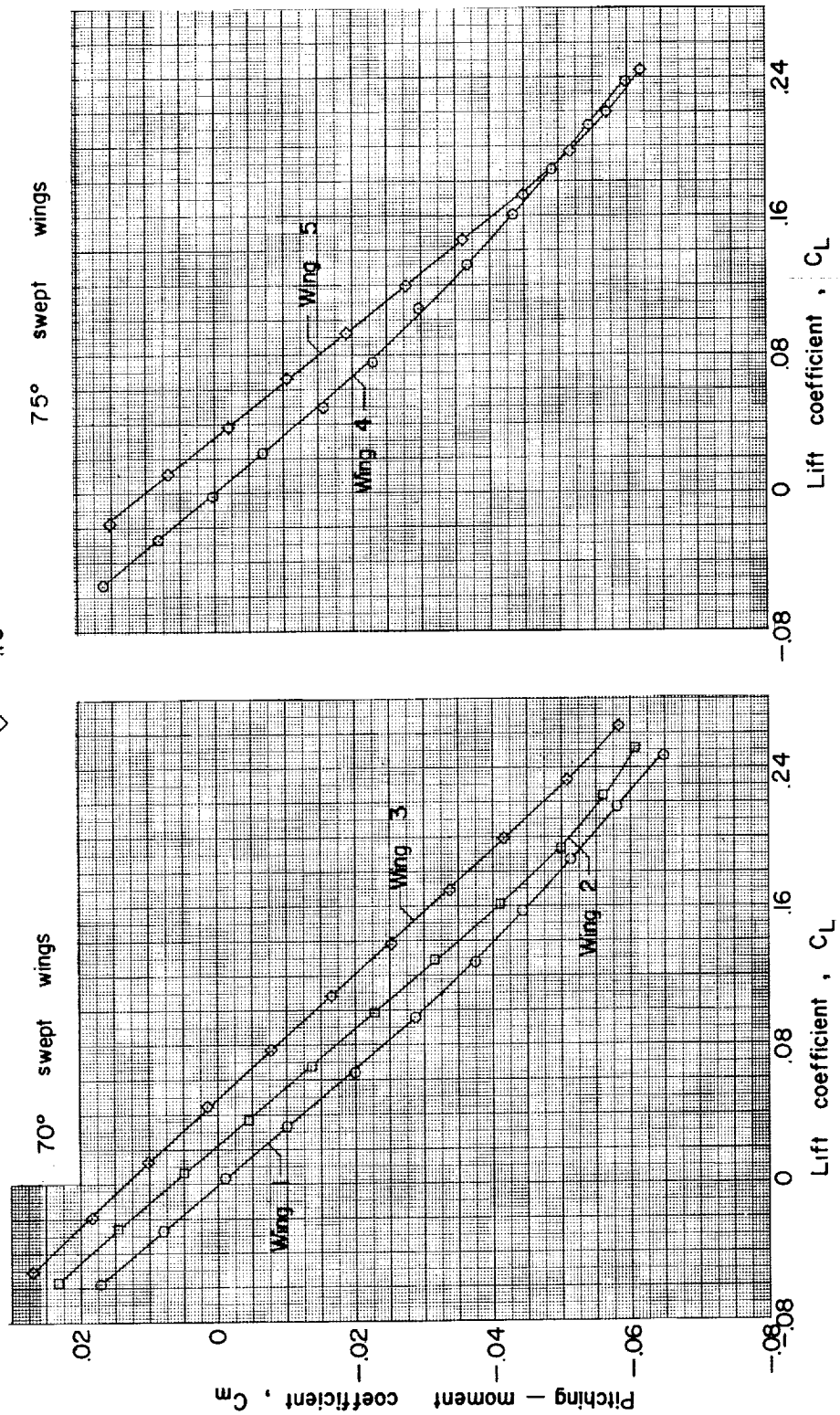

(d) Pitching-moment coefficient as a function of lift coefficient.

Figure 6.- Continued.

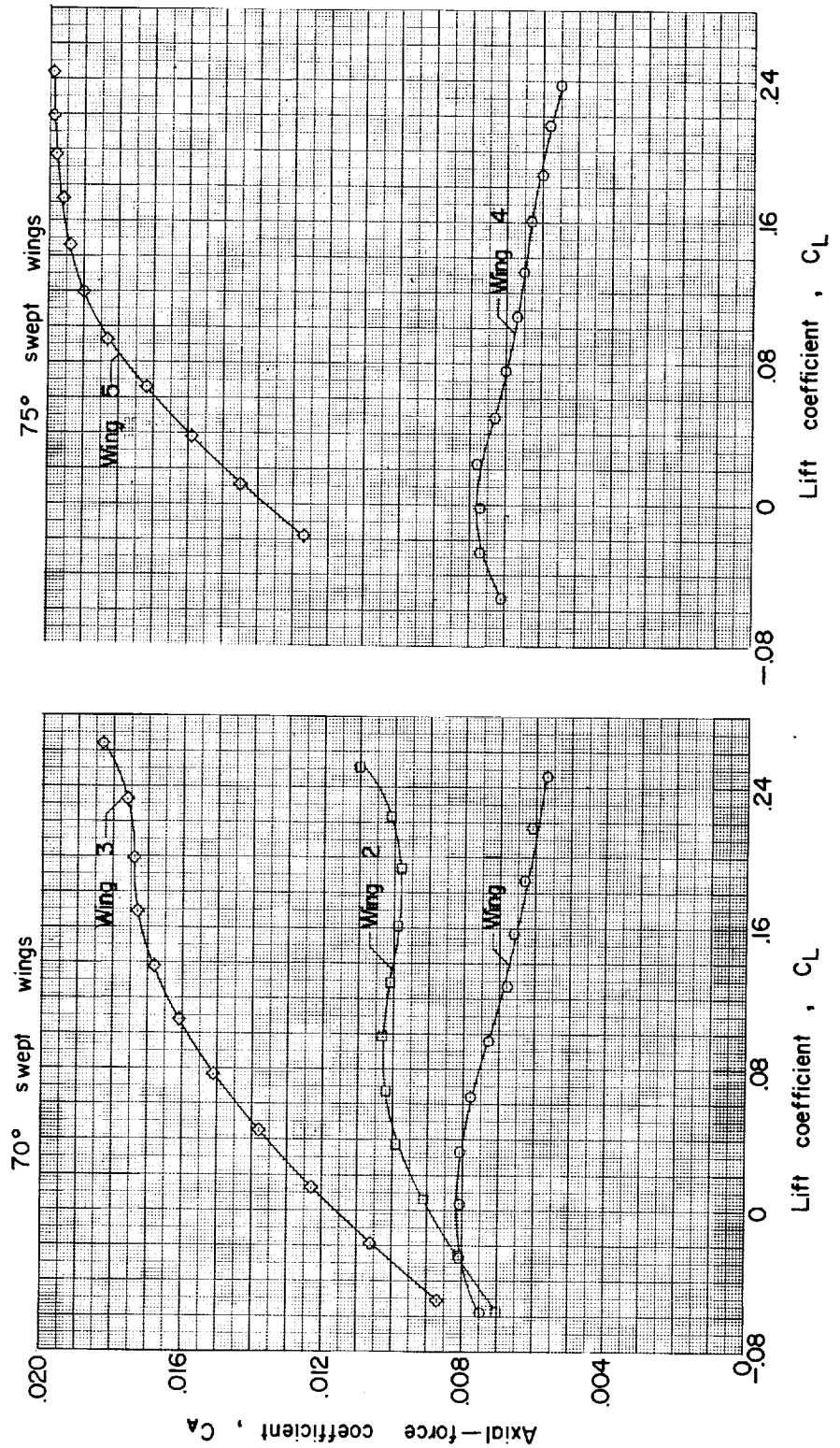

(e) Axial-force coefficient as a function of lift coefficient.

Figure 6.- Concluded.

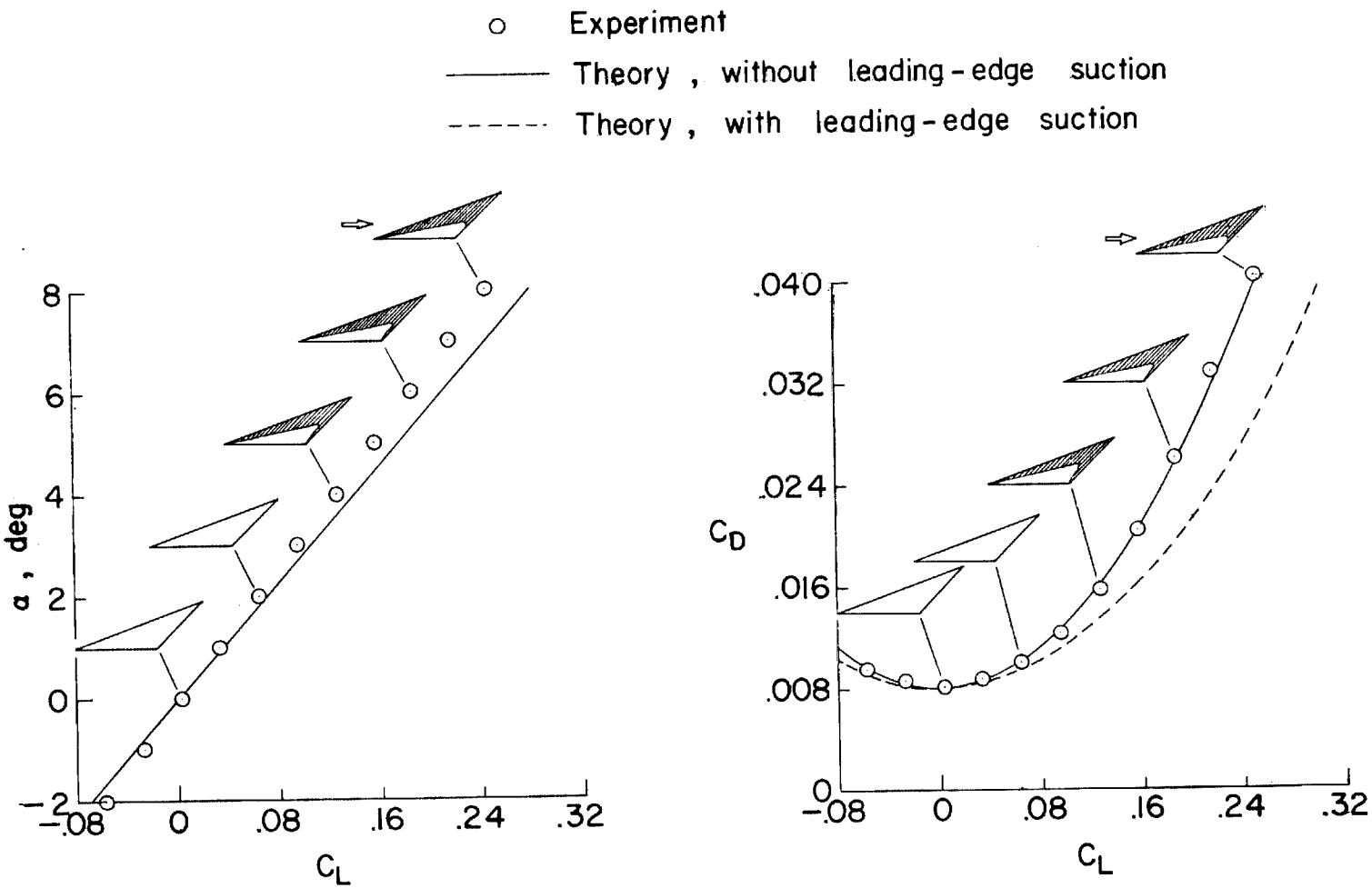

(a) Wing 1. $\Lambda = 70^\circ$; $C_{L,design} = 0$.

Figure 7.- Comparison of theoretical and experimental aerodynamic characteristics. Shaded areas on the sketches indicate regions of separated flow on the wing upper surface.

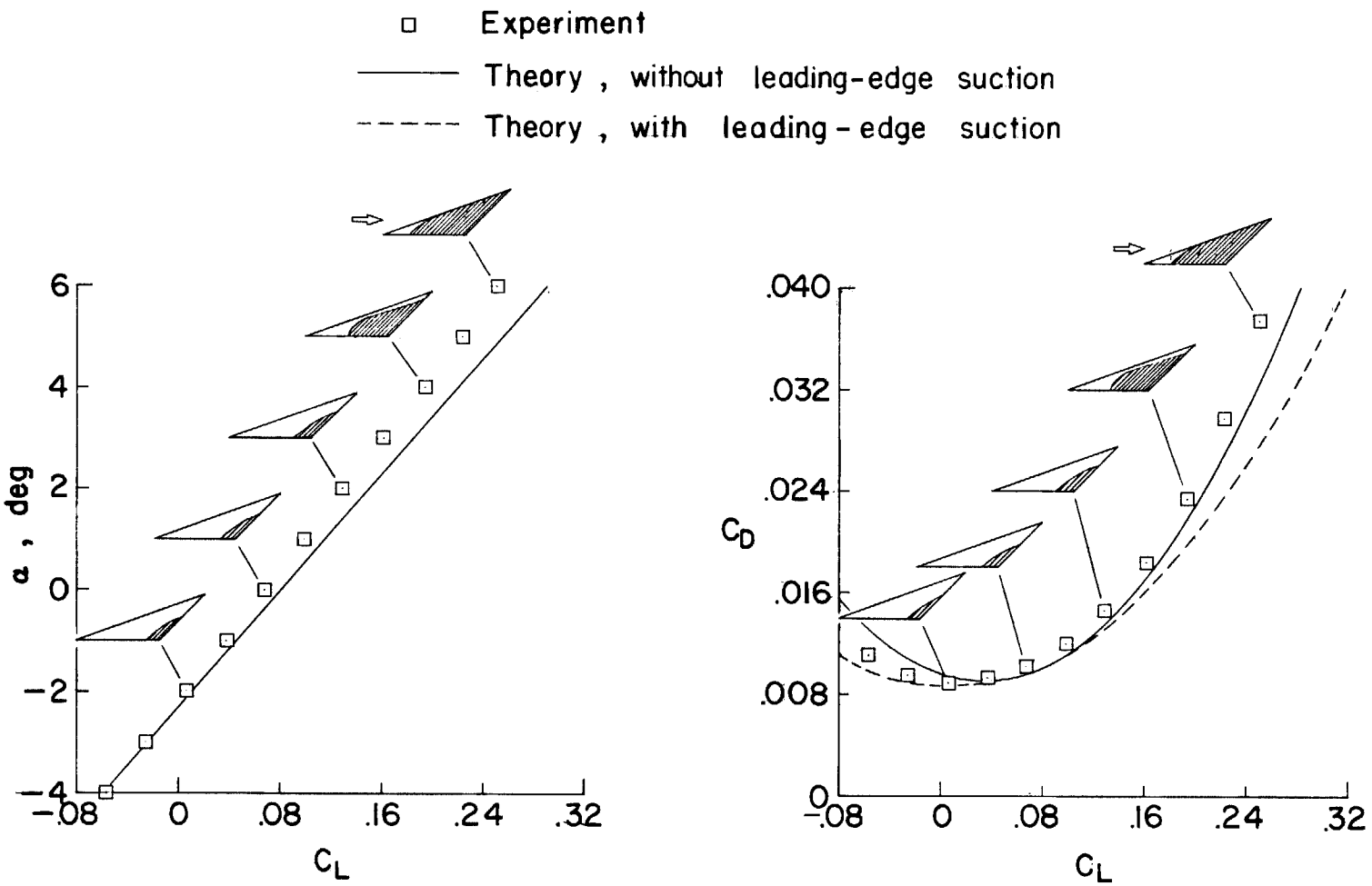

(b) Wing 2. $\Lambda = 70^\circ$; $C_{L,design} = 0.08$.

Figure 7.- Continued.

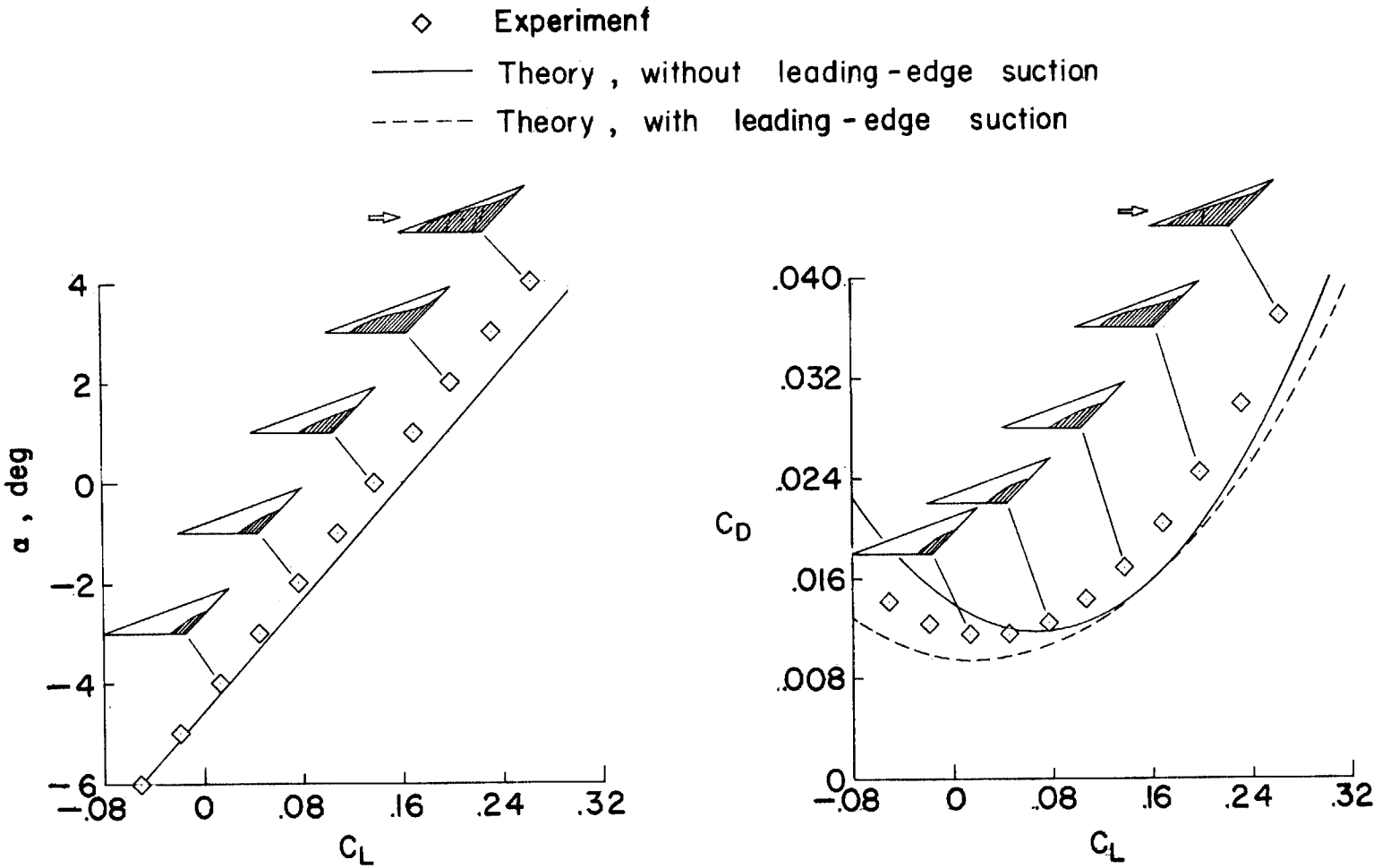

(c) Wing 3. $\Lambda = 70^{\circ}$; $C_{L,design} = 0.16$.

Figure 7.- Continued.

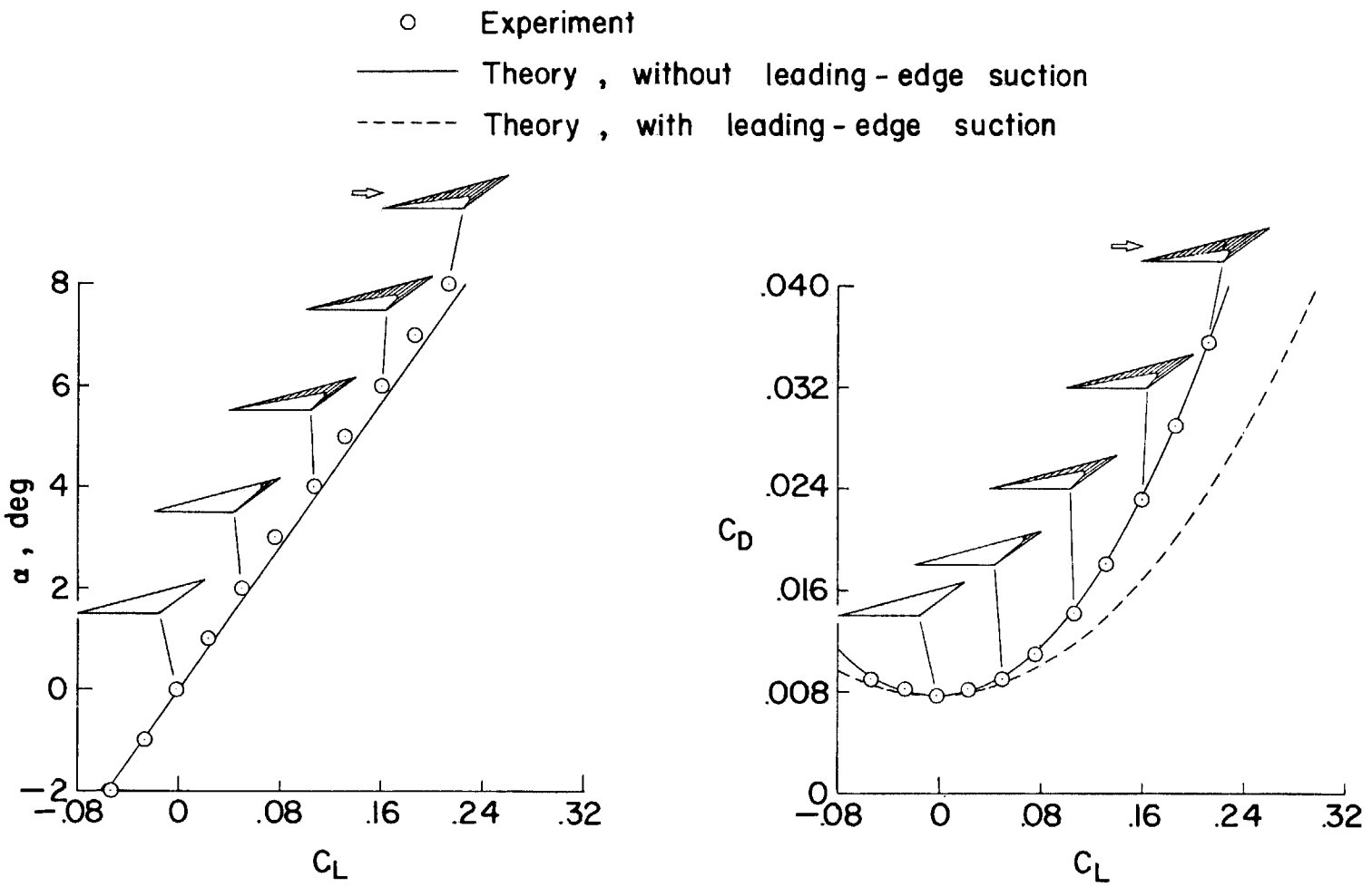

(d) Wing 4. $\Lambda = 75^{\circ}$; $C_{L,design} = 0$.

Figure 7.- Continued.

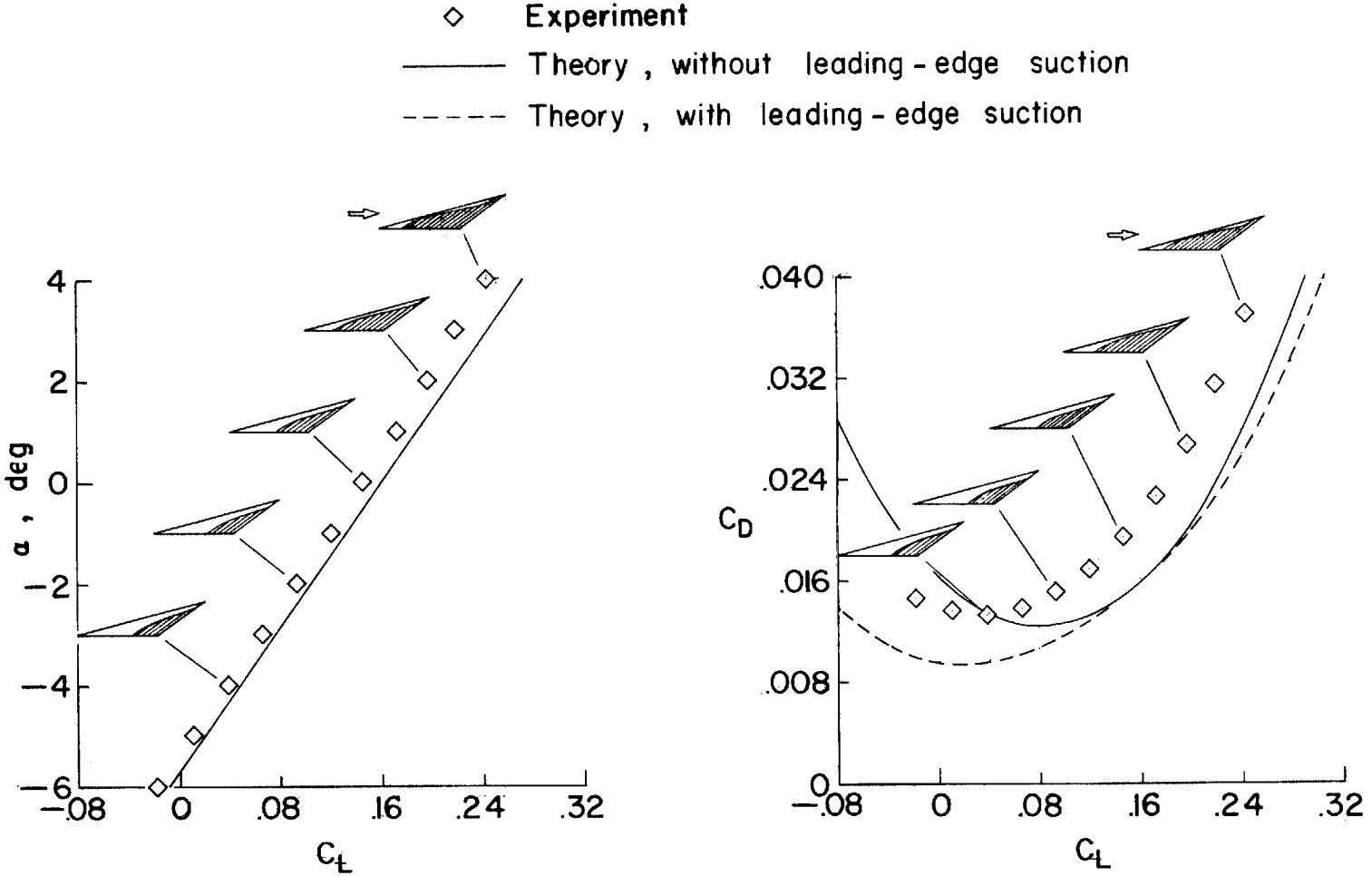

(e) Wing 5. $\Lambda = 75^\circ$; $C_{L,design} = 0.16$.

Figure 7.- Concluded.

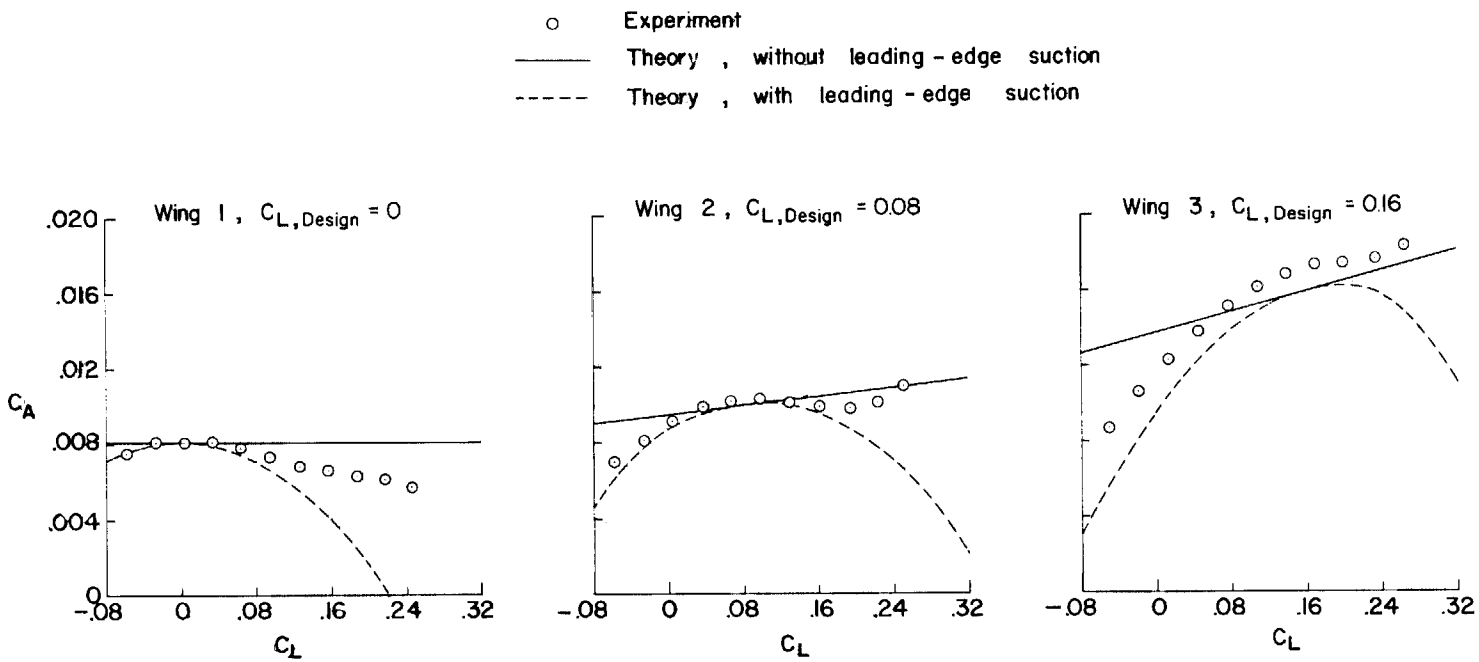

(a) 70° swept wings.

Figure 8.- Comparison of theoretical and experimental variation of axial-force coefficient with lift coefficient.

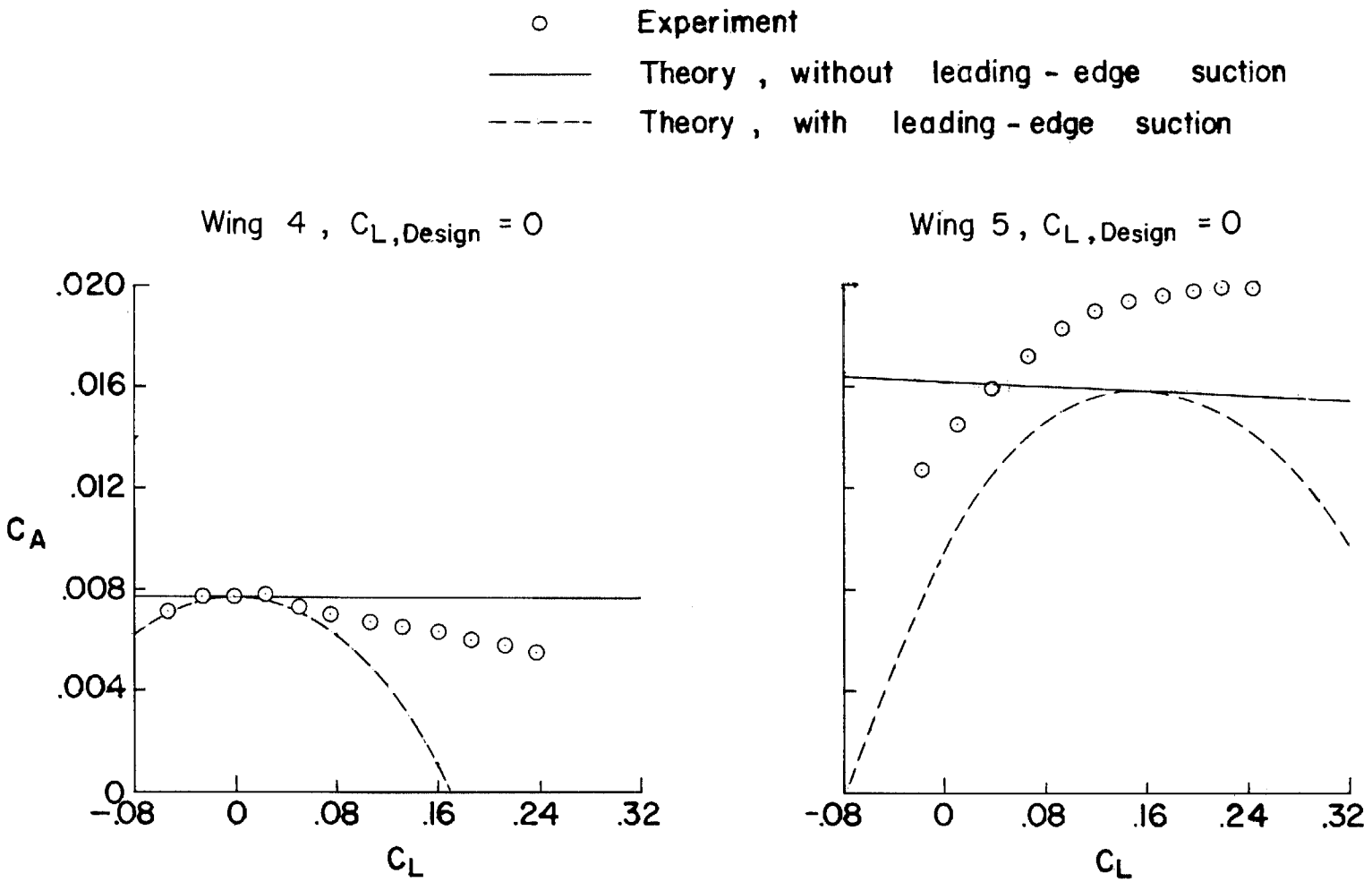

(b) 75° swept wings.

Figure 8.- Concluded.

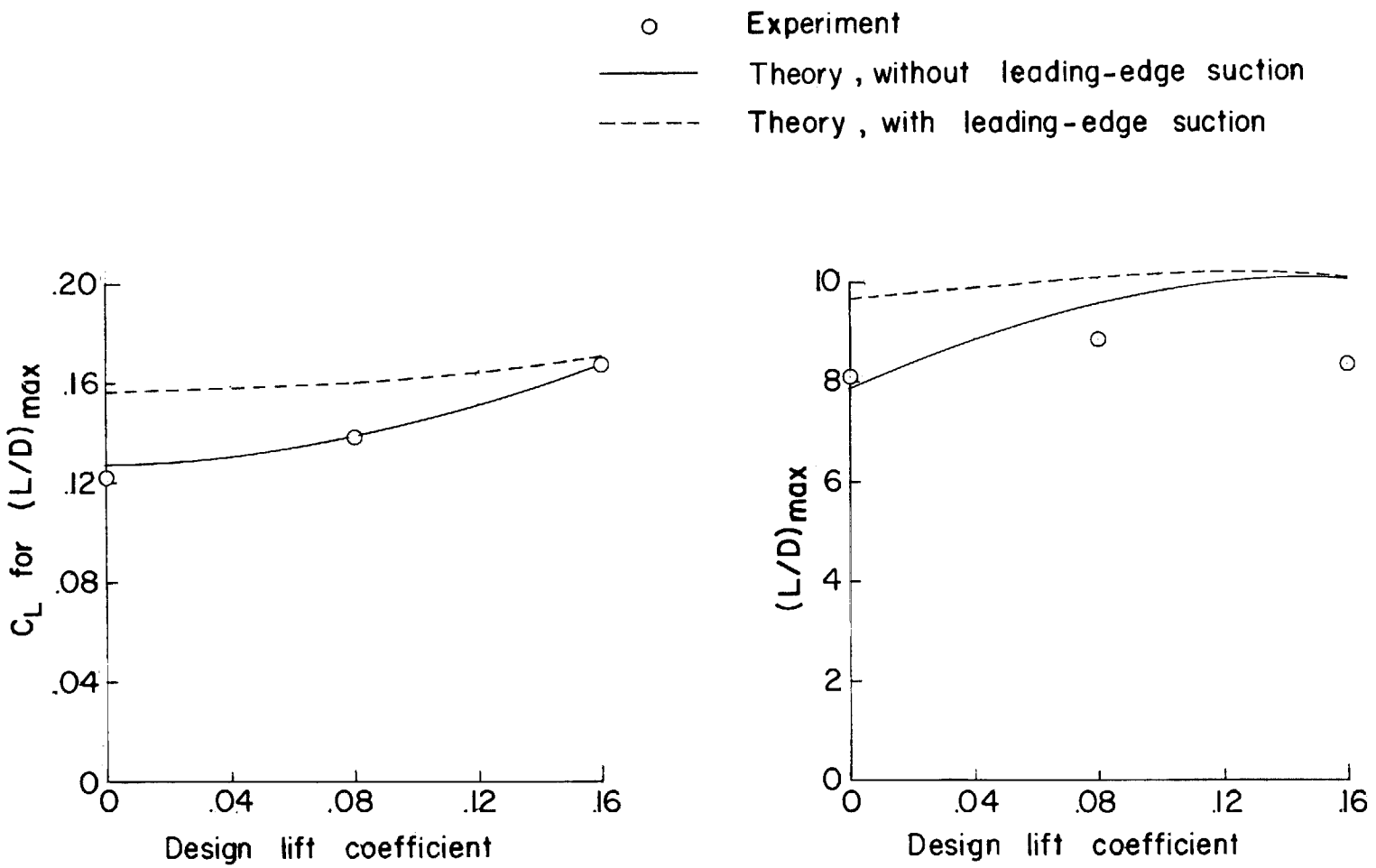

(a) 70° swept wings.

Figure 9.- Optimum lift coefficient and maximum lift-drag ratio as a function of design lift coefficient (degree of twist and camber).

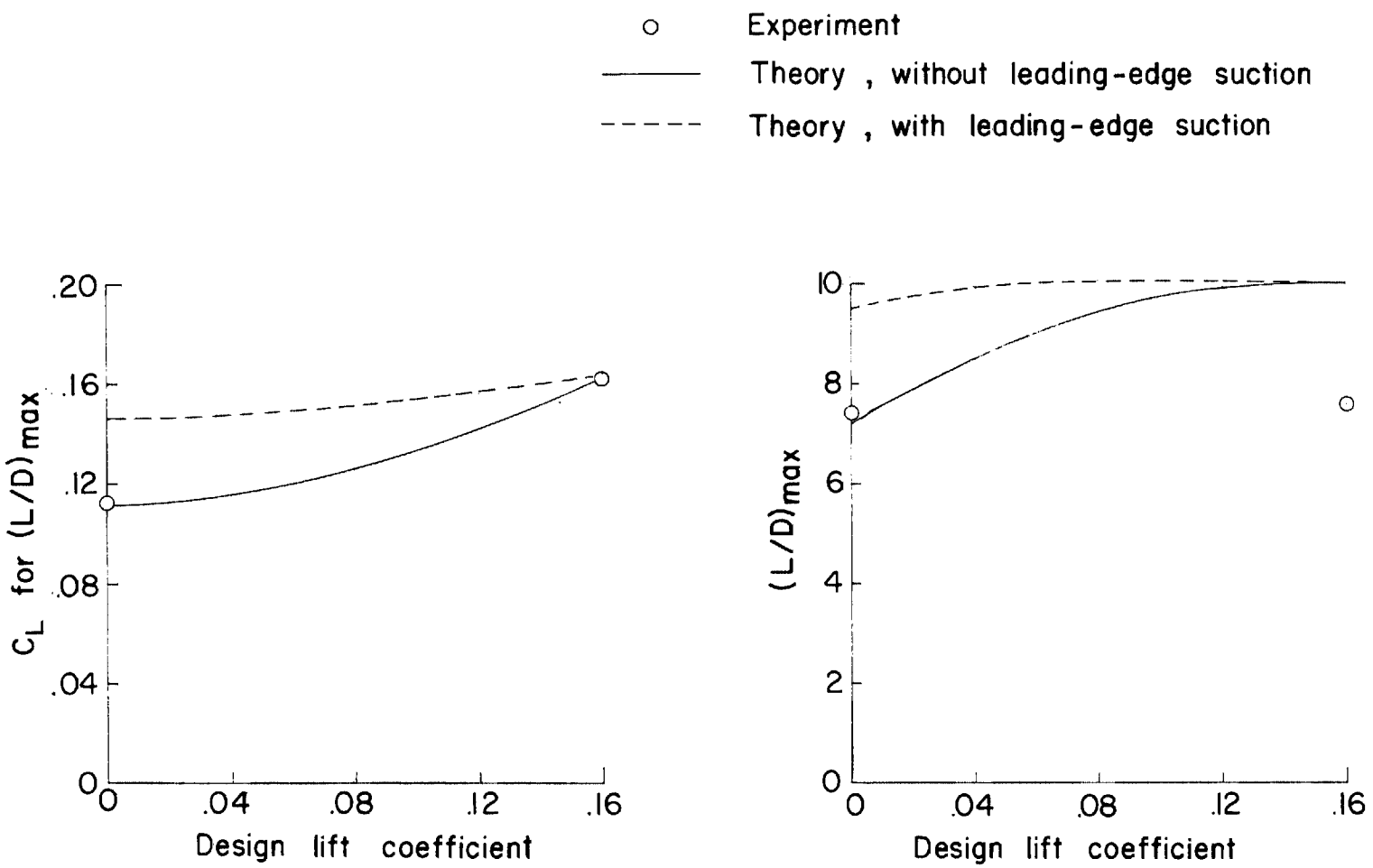

(b) 75° swept wings.

Figure 9.- Concluded.

NASA - Langley Field, Va. L-876